


A Liquid Chromatography with Tandem Mass Spectrometry-Based Proteomic Analysis of the Proteins Secreted by Human Adipose-Derived Mesenchymal Stem Cells

Cell Transplantation
2018, Vol. 27(10) 1469–1494
© The Author(s) 2018
Article reuse guidelines:
sagepub.com/journals-permissions
DOI: 10.1177/0963689718795096
journals.sagepub.com/home/ct


Yoshiki Nakashima¹, Saifun Nahar², Chika Miyagi-Shiohira¹, Takao Kinjo³, Zensei Toyoda³, Naoya Kobayashi⁴, Issei Saitoh⁵, Masami Watanabe⁶, Jiro Fujita², and Hirofumi Noguchi¹ 

Abstract

Liquid chromatography using a tandem mass spectrometer (LC-MS/MS) is a method of proteomic analysis. A shotgun analysis by LC-MS/MS comprehensively identifies proteins from tissues and cells with high resolution. The hepatic function of mice with acute hepatitis following the intraperitoneal administration of CCL4 was improved by the tail vein administration of the culture conditional medium (CM) of human mesenchymal stem cells from adipose tissue (hMSC-AT). In this study, a secreted protein expression analysis of hMSC-AT was performed using LC-MS/MS; 128 proteins were identified. LC-MS/MS showed that 106 new functional proteins and 22 proteins (FINC, PAII, POSTN, PGS2, TIMP1, AMPN, CFAH, VIME, PEDF, SPRC, LEG1, ITGBL, ENOA, CSPG2, CLUS, IBP4, IBP7, PGS1, IBP2, STC2, CTHRI, CD9) were previously reported in hMSC-AT-CMs. In addition, various proteins associated with growth (SAP, SEM7A, PTK7); immune system processes (CO1A2, CO1A1, CATB, TSPI, GAS6, PTX3, C1S, SEM7A, G3P, PXDN, SRCRL, CD248, SPON2, ENPP2, CD109, CFAB, CATLI, MFAP5, MIF, CXCL5, ADAM9, CATK); and reproduction (MMP2, CATB, FBLN1, SAP, MFGM, GDN, CYTC) were identified in hMSC-AT-CMs. These results indicate that a comprehensive expression analysis of proteins by LC-MS/MS is useful for investigating new factors associated with cellular components, biological processes, and molecular functions.

Keywords

Human mesenchymal stem cells from adipose tissue (hMSC-AT), acute hepatitis, conditional medium (CM), LC-MS/MS analysis

Introduction

The clinical application of liver cell therapy using stem cells has great significance. The liver can develop acute hepatitis or chronic liver failure due to the influence of factors such as drugs, xenobiotics, and viruses. Eventually, chronic hepatitis and fibrosis develop and the ability to regenerate hepatocytes is lost¹. At present, the only effective treatment is liver transplantation; however, liver transplantation is associated with problems such as rejection and limitation of donors. Thus, alternative approaches are necessary, and stem cells are attracting attention as a therapeutic approach. Mesenchymal stem cells (MSCs) represent an outstanding candidate stem cell for clinical treatment. MSCs have been collected from various organs, including the bone marrow (BM)², cord blood³, placenta⁴, and adipose tissue (AT)^{5,6}. Currently, attention is being given to adipose tissue as a source of MSCs

¹ Department of Regenerative Medicine, Graduate School of Medicine, University of the Ryukyus, Okinawa, Japan

² Department of Infectious, Respiratory, and Digestive Medicine, Graduate School of Medicine, University of the Ryukyus, Okinawa, Japan

³ Department of Basic Laboratory Sciences, School of Health Sciences in Faculty of Medicine, University of the Ryukyus, Okinawa, Japan

⁴ Okayama Saidaiji Hospital, Okayama, Japan

⁵ Division of Pediatric Dentistry, Graduate School of Medical and Dental Science, Niigata University, Niigata, Japan

⁶ Department of Urology, Okayama University Graduate School of Medicine, Dentistry and Pharmaceutical Sciences, Okayama, Japan

Submitted: January 16, 2018. Revised: July 25, 2018. Accepted: July 26, 2018.

Corresponding Author:

Hirofumi Noguchi, MD, PhD, Department of Regenerative Medicine, Graduate School of Medicine, University of the Ryukyus, 207 Uehara, Nishihara, Okinawa 903-0215, Japan.

Email: noguchih@med.u-ryukyu.ac.jp



for regenerative medicine⁵⁻⁷. Adipose tissue contains large amounts of MSCs (adipose-derived mesenchymal stem cells (ADSCs)) and is considered to be a useful source of cells for clinical application because of its fast proliferation and high cellular activity.

In recent years, treatment methods using conditional medium of mesenchymal stem cells (MSC-CM) have been reported⁸⁻¹¹. Because the culture supernatant does not contain cellular components, there is a high possibility that they will have clinical applications because of the extremely low risk of complications (i.e. pulmonary embolism) associated with the administration of cells in the blood and canceration of the administered cells. Proteins are important components in the regulation of cellular functions such as cell proliferation, cell death, and the immune function, and in the induction of differentiation. Thus, proteomic analyses, which detect the expression of protein, are considered to be a powerful tool for analyzing the system biology and exploring the active factors in MSC-CMs.

Liquid chromatography by tandem mass spectrometry (LC-MS/MS) is an analytical chemistry technique that combines the physical separation capability of liquid chromatography (or high-performance liquid chromatography (HPLC)) and the mass spectrometric ability of mass spectrometry¹². MS involves a mass separation step; the ionized component is detected as it is. In soft ionization methods such as electrospray ionization (ESI)¹³⁻¹⁵, molecular weight-related ions are mainly detected (mass spectrum). In tandem mass spectrometry (MS/MS), specific ions are first selected by a mass separator (MS1). In addition, the fragmentation of ions occurs due to the collision of ions with inert gas. The fragment ions obtained are separated and detected by a second mass separator (MS2) (product ion spectrum). Molecular weight-related ions are mainly detected by MS, and precursor ions and product ions are detected by MS/MS. LC-MS/MS allows for the identification of proteins fragmented into peptides by trypsin. Our protocol was based on the bottom-up strategy of a proteomic MS analysis. Enzymatic digestion was carried out using the Filter Aided Sample Preparation (FASP) method with trypsin as protease¹⁶. The peptide mixture was treated with ZipTip and then on-line coupled nano-liquid chromatography (nano LC) was performed using an Orbitrap Elite Hybrid Mass Spectrometer (Thermo Fisher Scientific, Tokyo, Japan). In addition, an on-line LC-MS/MS system for quantitative proteomics based on data-dependent protein IDs and shotgun-based quantitative proteomics methods was used.

This study was performed to identify functional protein components in the conditional medium of human mesenchymal stem cells from adipose tissue (hMSC-AT-CM) using LC-MS/MS. The identification of the secreted protein components of hMSC-AT and protein components with therapeutic effects is expected to be useful for future cell therapy.

Materials and Methods

Reagents

The MSCGM-CD™ Mesenchymal Stem Cell Growth Medium BulletKit™ was obtained from Lonza (Basel, Switzerland). hMSC-ATs (46-year-old Caucasian female) (PromoCell, Heidelberg, Germany) were cultured. Fetal bovine serum (FBS) was obtained from BioWest (Nuaille, France). D-MEM/Ham's F-12 medium was obtained from Wako (Osaka, Japan). Plastic dishes were obtained from TPP (Trasadingen, Switzerland). All other materials used were of the highest commercial grade.

Flow Cytometry

Cell flow cytometry was performed using a NovoCyte® Flow Cytometer (ACEA Biosciences, Inc., San Diego, CA, USA) according to the manufacturer's instructions. Briefly, hMSC-ATs (1×10^5 cells) were mixed into 0.5 mL of Perfusion Solution (CORNING, Manassas, VA, USA). Each antibody (1/100 of the volume) was added to the cell admixture, which was then incubated on ice for 30 minutes. After washing the cells with Brilliant Stain Buffer (BD Biosciences, Franklin Lakes, NJ, USA), fluorescence activated cell sorting (FACS) measurement was carried out. The following primary antibodies were used: APC Mouse Anti-Human CD29, BV421 Mouse Anti-Human CD44, BV421 Mouse IgG2b κ Isotype Control, APC Mouse IgG1 κ Isotype Control (BD Biosciences, Franklin Lakes, NJ, USA); FITC anti-human CD90 (Thy1) Antibody, FITC Mouse IgG1 κ Isotype Ctrl Antibody, PerCP anti-human CD34 Antibody, PerCP Mouse IgG1 κ Isotype Ctrl Antibody, PE/Cy7 anti-human CD45 Antibody, and PE/Cy7 Mouse IgG1 κ Isotype Ctrl Antibody (BioLegend, Inc., San Diego, CA, USA).

Animal Care

All experimental protocols were in accordance with the guidelines for the care and use of laboratory animals set by Research Laboratory Center, Faculty of Medicine and the Institute for Animal Experiments, Faculty of Medicine, University of the Ryukyus (Okinawa, Japan). The experimental protocol was approved by the Committee on Animal Experiments of University of the Ryukyus (permit number: A2017101). C57BL/6 male mice (8-week-old; Japan SLC, Shizuoka, Japan) were maintained under controlled temperature ($23 \pm 2^\circ\text{C}$) and light conditions (lights on from 08:30–20:30). Animals were fed standard rodent chow pellets with ad libitum access to water. All efforts were made to minimize the suffering of the animals.

Preparation of the Mouse Model of Acute Liver Failure

Carbon tetrachloride (CCL4) (Wako 035-01273) diluted with olive oil (Wako 150-00276) was administered

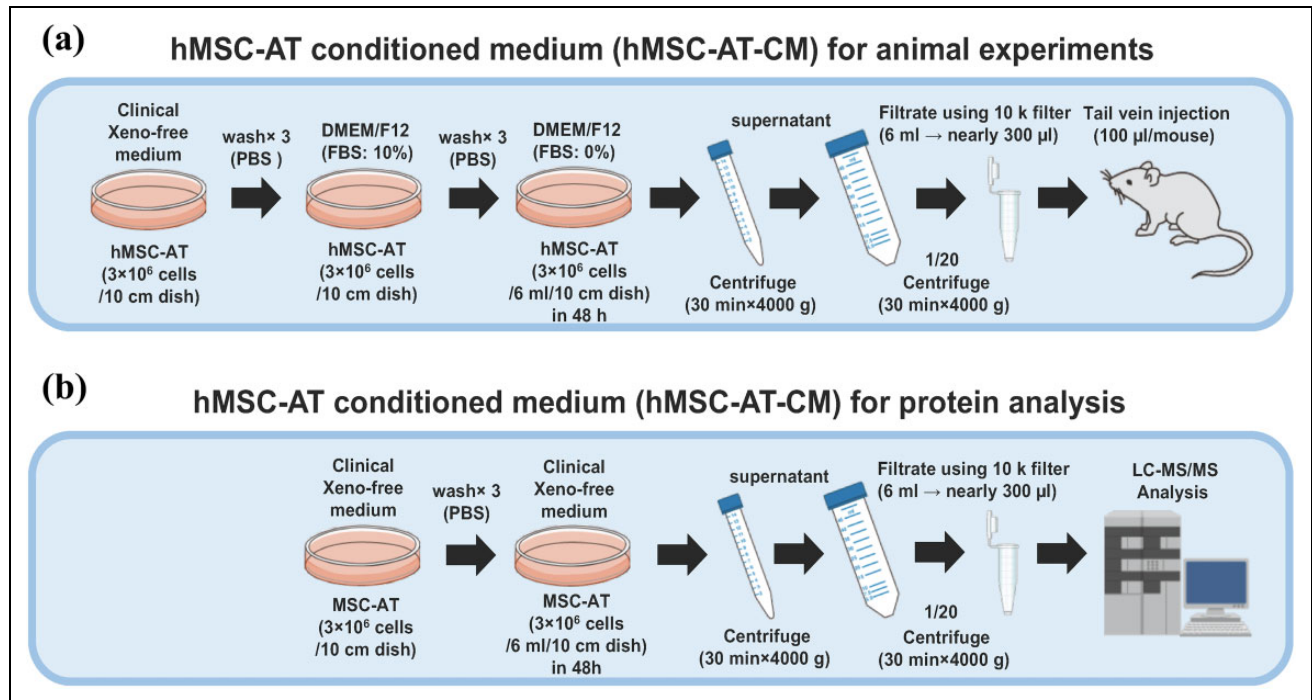


Fig. 1. Illustration of the preparation of conditional medium for hMSC-AT. (a) The procedure for administering 100 μL hMSC-AT-CM concentrate to the tail vein of the mouse. (b) The procedure for preparing the hMSC-AT-CM concentrate for the LC-MS/MS analysis.

intraperitoneally (0.5 mL/kg) to 8-week-old C57BL/6 male mice as a mouse model of acute liver failure. Nine mice each were used for both treated and control animals. At 4 h after the administration of CCL₄, 20-fold concentrated culture supernatant was administered via the mouse tail vein (100 μL of PBS and hMSC-AT-CM solution was administered via the mouse tail vein). Blood and liver tissues were sampled at 24 h after the administration of CCL₄. Under anesthesia, approximately 500 μL of blood was collected from the descending aorta using a 1 mL syringe (22 G injection needle) passed through heparin, centrifuged (150 g, 30 min, 4°C) after the coagulation, 100 μL of blood was obtained. Four hundred microliters of physiological saline were added to 100 μL of serum and diluted, and the blood components were analyzed (commissioned to SRL). The liver was fixed in formalin after sampling and HE staining was performed after the preparation of tissue sections. Fragmented DNA generated during apoptosis was detected by a TdT-mediated dUTP nick end-labeling (TUNEL) assay to identify apoptotic cells in the liver tissue. TUNEL staining was performed using the In Situ Apoptosis Detection kit (Takara Bio Inc., Shiga, Japan) and visualized using DAB as the chromogen. The Ki67 protein present in the nucleus of cells in G₁, S, G₂, M cycles (cell growth phase) was detected by using immunostaining in order to identify cells in the growth phase in liver tissue. The reagent Histofine Simple Stain MAX PO (Rabbit) (NICHIRE BIOSCIENCES INC., Tokyo, Japan) and anti-Ki67 antibody (ab 15580) (Abcam, Cambridge, UK) were used.

Preparations of hMSC-AT-CMs for Animal Studies and the Analysis of the Protein Expression by LC-MS/MS

The hMSCs used in this study are limited to three to five passages in order to match the cell nature with clinically used hMSCs. Two milliliters of DMEM/F12 medium was added to hMSC-AT (1×10^6 cells) and cultured for 48 h to prepare hMSC-AT-CMs; this was concentrated to 1/20 of the original volume using a 10 k filter, 100 μL was injected per mouse. The 20-fold concentrated hMSC-AT-CM was serous and successfully passed through a 32 G injection needle (Fig. 1(a)). Two milliliters of clinical Xeno-free medium (MSCGM-CD mesenchymal stem cell BulletKit [Lonza]) was added to hMSC-AT (1×10^6 cells) and cultured for 48 h to prepare hMSC-AT-CMs and then concentrated to 1/20 of the original volume using a 10 k filter, after which the component proteins were analyzed by LC-MS/MS. Twenty-fold concentrated hMSC-AT-CM was subjected to LC-MS/MS. If the medium's albumin concentration is high, the accuracy of a protein analysis decreases. Thus, after washing these cells with phosphate buffered saline (PBS), they were cultured in albumin-free medium and the resulting culture supernatant was used for this study (Fig. 1(b)). One hundred twenty-eight proteins were identified from the hMSC-AT-CM samples; the identified proteins are listed in Table 1. In this study, DMEM/F12 (containing 0% FBS) was used to prepare hMSC-AT-CMs to be administered to mice, due to the difficulty of accurately observing the therapeutic effect of hMSC-AT-secreted protein when the

Table 1. Details of the hMSC-AT Secreted Protein Identified.

UniProt/SWISS-PROT ID	Description	Protein score ^a	Protein mass (kDa)	Protein	pl ^b	Num. of matches ^c	Num. of significant matches ^d	Num. of sequences ^e	Num. of significant sequences ^f	Num. of unique sequences ^g	Sequence coverage ^h	emPAI ⁱ
FINC_HUMAN	Fibronectin	17,045	262,460		5.46	1127	667	120	99	53	0.67	7.1
BGH3_HUMAN	Transforming growth factor-beta-induced protein ig-h3	5287	74,634		7.62	161	135	26	18	26	0.61	2.83
CO6A1_HUMAN	Collagen alpha-1(VI) chain	4997	108,462		5.26	168	126	33	25	33	0.49	1.83
CO6A3_HUMAN	Collagen alpha-3(VI) chain	4217	343,457		6.26	224	169	85	66	85	0.41	1.32
CO1A2_HUMAN	Collagen alpha-2(I) chain	3164	129,235		9.08	209	129	51	38	46	0.63	2.65
PA11_HUMAN	Plasminogen activator inhibitor 1	2264	45,031		6.68	95	59	19	12	19	0.56	2.64
FSTL1_HUMAN	Follistatin-related protein 1	1973	34,963		5.39	50	38	13	10	13	0.53	2.69
POSTN_HUMAN	Periostin	1936	93,255		7.27	146	83	41	32	41	0.62	4.49
MMP2_HUMAN	72 kDa type IV collagenase	1619	73,835		5.26	106	66	25	23	15	0.65	3.35
CO1A1_HUMAN	Collagen alpha-1(I) chain	1576	138,857		5.6	206	87	36	28	27	0.44	1.47
FBN1_HUMAN	Fibrillin-1	1557	312,022		4.81	95	54	46	27	43	0.29	0.44
FBN2_HUMAN	Fibrillin-2	1479	314,558		4.73	106	54	55	25	52	0.38	0.4
CATB_HUMAN	Cathepsin B	1327	37,797		5.88	46	31	12	9	12	0.56	2.35
LAMB1_HUMAN	Laminin subunit beta-1	1302	197,909		4.83	62	43	29	19	29	0.35	0.5
PGS2_HUMAN	Decorin	1223	39,722		8.75	28	18	9	4	9	0.36	0.69
CO6A2_HUMAN	Collagen alpha-2(VI) chain	1144	108,512		5.85	79	56	23	14	23	0.32	0.78
LTBP1_HUMAN	Latent-transforming growth factor beta-binding protein 1	1125	186,673		5.63	77	53	31	21	22	0.31	0.71
TSPI_HUMAN	Thrombospondin-1	1023	129,300		4.71	56	39	22	14	20	0.28	0.68
TIMP1_HUMAN	Metalloproteinase inhibitor 1	961	23,156		8.46	58	43	7	6	7	0.54	2.48
AMPN_HUMAN	Aminopeptidase N	896	109,471		5.31	23	17	10	5	10	0.17	0.21
CO3A1_HUMAN	Collagen alpha-1(III) chain	868	138,479		6.21	57	30	24	14	22	0.24	0.57
CFAH_HUMAN	Complement factor H	790	139,005		6.21	41	28	20	15	20	0.3	0.57
LTBP2_HUMAN	Latent-transforming growth factor beta-binding protein 2	765	194,923		5.06	54	28	26	15	26	0.26	0.38
CO5A1_HUMAN	Collagen alpha-1(V) chain	664	183,447		4.94	32	19	12	6	11	0.12	0.15
LG3BP_HUMAN	Galectin-3-binding protein	640	65,289		5.13	29	21	10	7	10	0.32	0.56
LAMC1_HUMAN	Laminin subunit gamma-1	590	177,489		5.01	54	31	28	15	28	0.3	0.42
MFAP2_HUMAN	Microfibrillar-associated protein 2	579	20,812		4.86	11	10	3	3	3	0.21	0.81
VIME_HUMAN	Vimentin	531	53,619		5.06	36	16	14	7	14	0.37	0.86
PCOC1_HUMAN	Procollagen C-endopeptidase enhancer 1	522	47,942		7.41	47	23	17	11	17	0.63	1.84
COBAl_HUMAN	Collagen alpha-1(XI) chain	513	180,954		5.06	26	16	12	4	11	0.17	0.12
PEDF_HUMAN	Pigment epithelium-derived factor	497	46,283		5.97	15	13	9	7	9	0.3	0.88
SPRC_HUMAN	SPARC	435	34,610		4.73	40	25	13	9	6	0.63	2.32
GAS6_HUMAN	Growth arrest-specific protein 6	433	79,625		5.84	19	12	9	5	9	0.24	0.3
LEGI_HUMAN	Galectin-1	420	14,706		5.34	12	11	3	3	3	0.32	1.31
OLF3_HUMAN	Olfactomedin-like protein 3	390	45,981		6.17	24	14	10	6	10	0.36	0.72
PTX3_HUMAN	Pentraxin-related protein PTX3	381	41,949		4.94	33	21	12	10	12	0.42	1.7
LAMA2_HUMAN	Laminin subunit alpha-2	364	343,684		6.01	39	13	27	8	27	0.17	0.1
ITGBL_HUMAN	Integrin beta-like protein 1	361	53,884		5.39	24	15	14	9	14	0.38	1.01

(continued)

Table 1. (continued)

UniProt/SWISS-PROT ID	Description	Protein score ^a	Protein mass (kDa)	pI ^b	Num. of matches ^c	Num. of significant matches ^d	Num. of sequences ^e	Num. of significant sequences ^f	Num. of unique sequences ^g	Sequence coverage ^h	emPAI ⁱ
AEBP1_HUMAN	Adipocyte enhancer-binding protein 1	361	130,847	5.05	9	7	5	4	5	0.07	0.14
CO5A2_HUMAN	Collagen alpha-2(V) chain	355	144,821	6.07	18	10	9	4	8	0.12	0.12
FBLN1_HUMAN	Fibulin-1	352	77,162	5.07	20	12	13	9	6	0.29	0.63
ENOA_HUMAN	Alpha-enolase	350	47,139	7.01	13	10	3	3	3	0.13	0.3
FBLN5_HUMAN	Fibulin-5	341	50,147	4.58	22	13	9	6	9	0.34	0.94
LUM_HUMAN	Lumican	311	38,405	6.16	35	12	11	5	11	0.37	0.72
DKK3_HUMAN	Dickkopf-related protein 3	290	38,365	4.59	9	8	4	4	4	0.25	0.54
CO4A2_HUMAN	Collagen alpha-2(IV) chain	285	167,449	8.89	11	8	4	3	4	0.05	0.08
GSPG2_HUMAN	Versican core protein	282	372,590	4.43	24	11	17	9	17	0.1	0.11
SRPX_HUMAN	Sushi repeat-containing protein SRPX	279	51,538	8.98	25	14	14	8	14	0.48	0.91
C1S_HUMAN	Complement C1 s subcomponent	272	76,635	4.86	27	13	14	8	14	0.35	0.55
ECM1_HUMAN	Extracellular matrix protein 1	268	60,635	6.25	39	16	17	9	17	0.41	0.86
NIDI_HUMAN	Nidogen-1	248	136,291	5.12	35	18	19	11	17	0.26	0.4
SAP_HUMAN	Prosaposin	242	58,074	5.06	18	12	10	4	10	0.28	0.33
SEM7A_HUMAN	Semaphorin-7A	229	74,776	7.57	21	12	15	10	15	0.37	0.85
CLUS_HUMAN	Clusterin	225	52,461	5.89	9	7	4	3	4	0.18	0.27
LYOX_HUMAN	Protein-lysine 6-oxidase	224	46,915	8.36	18	13	8	4	8	0.3	0.56
QSOX1_HUMAN	Sulfinyldryl oxidase 1	209	82,526	9.13	18	8	8	6	8	0.18	0.36
G3P_HUMAN	Glyceraldehyde-3-phosphate dehydrogenase	196	36,030	8.57	8	6	6	5	6	0.34	0.78
TIGN1_HUMAN	Testican-1	184	49,092	5.74	12	8	9	6	9	0.34	0.66
EMIL1_HUMAN	EMILIN-1	177	106,601	5.07	9	5	7	4	7	0.15	0.17
WISP2_HUMAN	WNT1-inducible-signaling pathway protein 2	168	26,807	8.32	11	4	5	2	5	0.35	0.36
TFPI_HUMAN	Tissue factor pathway inhibitor	164	34,992	8.61	24	3	2	1	2	0.13	0.13
PXDN_HUMAN	Peroxidasin homolog	164	165,170	6.79	18	6	10	4	10	0.12	0.11
PGBM_HUMAN	Basement membrane-specific heparan sulfate proteoglycan core protein	159	468,532	6.06	22	7	11	4	11	0.06	0.04
IBP4_HUMAN	Insulin-like growth factor-binding protein 4	149	27,915	6.81	16	6	10	5	10	0.52	1.1
VASN_HUMAN	Vasorin	145	71,668	7.16	8	7	4	4	4	0.09	0.26
GPNMB_HUMAN	Transmembrane glycoprotein NMB	141	63,882	6.17	5	4	2	1	2	0.06	0.07
SRCL_HUMAN	Soluble scavenger receptor cysteine-rich domain-containing protein SSC5D	140	165,639	5.71	26	3	4	1	4	0.04	0.03
FBLN3_HUMAN	EGF-containing fibulin-like extracellular matrix protein 1	138	54,604	4.95	21	9	10	4	10	0.32	0.36
PLTP_HUMAN	Phospholipid transfer protein	137	54,705	6.53	8	4	4	2	4	0.16	0.16
PROFI_HUMAN	Profilin-1	135	15,045	8.44	5	4	3	2	3	0.31	0.72
IBP7_HUMAN	Insulin-like growth factor-binding protein 7	134	29,111	8.25	12	7	5	3	5	0.3	0.53
PGSI_HUMAN	Biglycan	133	41,628	7.16	10	4	6	3	6	0.27	0.35
NUCB1_HUMAN	Nucleobindin-1	124	53,846	5.15	20	5	14	4	14	0.45	0.36
CD44_HUMAN	CD44 antigen	119	81,487	5.13	8	4	3	1	3	0.08	0.05
AGRIN_HUMAN	Agrin	114	217,092	6.01	10	4	7	4	7	0.09	0.08
MFGM_HUMAN	xLactadherin	111	43,095	8.47	16	6	6	3	6	0.2	0.34

(continued)

Table 1. (continued)

UniProt/SWISS- PROT ID	Description	Protein score ^a	Protein mass (kDa)	pI ^b	Num. of matches ^c	Num. of significant matches ^d	Num. of sequences ^e	Num. of significant sequences ^f	Num. of unique sequences ^g	Sequence coverage ^h	emPAI ⁱ
RCN1_HUMAN	Reticulocalbin-1	111	38,866	4.86	3	2	1	1	1	0.06	0.11
FAM3C_HUMAN	Protein FAM3C	109	24,665	8.52	3	3	1	1	1	0.07	0.18
CATZ_HUMAN	Cathepsin Z	108	33,846	6.7	6	4	4	3	4	0.25	0.44
PDI1A1_HUMAN	Protein disulfide-isomerase	106	57,081	4.76	5	4	3	2	3	0.14	0.16
IBP2_HUMAN	Insulin-like growth factor-binding protein 2	104	34,791	7.48	7	4	5	3	5	0.27	0.43
TPPI_HUMAN	Tripeptidyl-peptidase I	103	61,210	6.01	3	2	2	1	2	0.08	0.07
GDN_HUMAN	Glia-derived nexin	99	43,974	9.35	16	5	8	4	8	0.28	0.46
CD248_HUMAN	Endostalin	93	80,807	5.18	5	4	3	3	3	0.09	0.17
SPON2_HUMAN	Spondin-2	92	35,824	5.35	26	8	12	7	12	0.44	1.25
MARCS_HUMAN	Myristoylated alanine-rich C-kinase substrate	91	31,536	4.47	3	2	2	1	2	0.1	0.3
LAMA1_HUMAN	Laminin subunit: alpha-1	90	336,867	5.93	17	3	11	3	11	0.08	0.04
SERP1_HUMAN	Serpin H1	90	46,411	8.75	15	5	6	2	6	0.2	0.2
PLOD1_HUMAN	Procollagen-lysine,2-oxoglutarate 5-dioxygenase 1	84	83,497	6.47	12	4	9	3	9	0.18	0.16
CO4A1_HUMAN	Collagen alpha-1(IV) chain	80	160,514	8.55	7	2	6	2	6	0.1	0.05
GOLM1_HUMAN	Golgi membrane protein 1	79	45,306	4.91	10	4	6	2	6	0.19	0.2
ENPP2_HUMAN	Ectonucleotide pyrophosphatase/ phosphodiesterase family member 2	78	98,930	7.14	11	6	8	4	8	0.17	0.18
LAMA4_HUMAN	Laminin subunit: alpha-4	77	202,397	5.89	15	3	11	3	11	0.11	0.06
TARSH_HUMAN	Target of Nesh-SH3	77	118,569	9.48	7	3	6	2	6	0.08	0.07
PTK7_HUMAN	Inactive tyrosine-protein kinase 7	75	118,317	6.67	3	2	3	2	3	0.04	0.07
SAP3_HUMAN	Ganglioside GM2 activator	73	20,825	5.17	6	3	3	2	3	0.4	0.48
CD109_HUMAN	CD109 antigen	72	161,587	5.59	12	1	6	1	6	0.06	0.03
PAMR1_HUMAN	Inactive serine protease PAMR1	70	80,146	7.57	5	2	5	2	5	0.16	0.11
KPYM_HUMAN	Pyruvate kinase PKM	68	57,900	7.96	7	3	4	3	4	0.16	0.24
PTGDS_HUMAN	Prostaglandin-H2 D-isomerase	64	21,015	7.66	3	1	2	1	2	0.17	0.22
IBP6_HUMAN	Insulin-like growth factor-binding protein 6	64	25,306	8.15	3	2	3	2	3	0.25	0.39

^a Protein score is calculated from the score of the peptide attributed to the protein; ^b pI: (Predicted) isoelectric point.; ^c Number of matches is spectrum number matched to protein#1; ^d Number of significant matches is spectrum number that matches protein and exceeds the identification criteria; ^e Number of sequences is number of peptides matched to protein#2; ^f Number of significant sequences is number of peptides exceeding the identification criteria matched to proteins; ^g Sequence coverage is the ratio of the total number of matched peptide residues to the total length of the protein; ^h Exponentially Modified Protein Abundance Index (http://www.matrixscience.com/help/quant_help.html).

Table 2. Sequences of Primers used for the RT-PCR.

Gnens	GenBank number	Forward primer (5'-3')	Reverse primer (5'-3')	Product size (bp)
human CD29	NM_002211.3	CTGAAGACTATCCCATTGACCTCTA	GCTAATGTAAGGCATCACAGTCTTT	179
human CD34	NM_001025109.1	CCTGCTCTCTTGTAATGATATAGCC	GAGACTAGAACTGAGCTGTTTGTCC	227
human CD44	NM_000610.3	ACTAGTGTTCAAGTGCCTCTTGTTT	GCCTCTTTTTGGGAATATCTAGAAG	227
human CD45	NM_001267798.1	TTCTTAGGGTAACAGAGGAGGAAAT	ACAAATACTTCTGTGTCCAGAAAGG	167
human HGF	NM_000601.5	ACAGTCATAGCTGAAGTAAGTGTGT	GCAGGATACATGGTGAAGAGAAATG	511
human SCAI	NM_001144877.2	CTTCACTCGTATTGCTGTGTCTCTA	GCATTGCACGTATTTACTATCCTCT	183
human VEGFA	NM_001025366.2	AAGTGGTGAAGTTCATGGATGTCTA	AAGTACGTTTCGTTAACTCAAGCTG	558
human GAPDH	NM_001256799.2	AGAAGTATGACAACAGCCTCAAGAT	CCAAATTCGTTGTCCATACCAGGAAA	544

protein component of clinical Xeno-free medium rich in growth factor proteins is concentrated.

Real-time PCR and RT-PCR

Five microliters of a cell admixture (concentration, 1×10^7 cells/ml) was collected. RNA was prepared for a qPCR using a SuperPrep Cell Lysis and RT kit according to the manufacturer's instructions (Toyobo Co., Ltd., Osaka, Japan). Quick Taq HS DyeMix was used according to the manufacturer's instructions (Toyobo Co., Ltd.). Real-time PCR analyses were performed using a LightCycler 96 Real-Time PCR system (Roche, Basel, Switzerland). The FastStart Essential DAN Green Master (Roche) was used according to the manufacturer's instructions. An RT-PCR was performed using a GeneAtlas 482 thermal cycler (Astec Co., Ltd., Fukuoka, Japan). Images were recorded using an Aplegen[®] Omega Lum C (Gel Company, San Francisco, CA, USA), and procedures were performed using the primers listed in Table 2.

Preparation of hMSC-AT

hMSC-ATs (46-year-old Caucasian female) were cultured (37°C, 5% CO₂) on a coated 100-mm culture plate (TPP 93100). The passage of cells was performed every 3 to 4 days after reaching 80% confluence after sowing the cells. The cells were washed with PBS (calcium, magnesium-free), and hMSC-ATs were dissociated using a dissociation solution. Subculturing was carried out by plating on uncoated 100-mm culture plate. An MSCGM-CD mesenchymal stem cell BulletKit (Lonza 00190632) was used for the culture medium. Trypsin/EDTA (Lonza CC-3232) was used for the dissociation solution.

Preparation of Culture Supernatant

hMSC-ATs were cultured on a 100 mm culture plate using an MSCGM-CD mesenchymal stem cell BulletKit (the number of cells was 3×10^6 /plate) until reaching 80% confluence. The cells were cultured for 24 h in D-MEM/Ham's F-12 medium (Wako 4230795) containing 10% FBS, after which the cells were washed with PBS (calcium,

magnesium-free); 2 ml of D-MEM/Ham's F-12 medium was then added to 1×10^6 cells and the cells were cultured for 48 h. After 48 h, the culture supernatant was aspirated with a pipette and centrifuged (1500 g, 30 minutes, 4°C) to remove the cells. After the centrifugation of the medium, the supernatant was concentrated 20 times using Amicon Ultra-15, PLGC Ultracell-PL membrane, 10 kDa (UFC901008) (MERCK, Kenilworth, NJ, USA) and a concentrated solution of culture supernatant was obtained.

Protein Identification by a Nano LC-MS/MS Analysis

A protein solution of 2066 µg/ml was obtained from the concentrated solution of culture supernatant. Finally, 0.4 µg of protein was used for nanoLC-MS/MS. The samples were analyzed via nano LC using an UltiMate 3000 RSLC nano system (Thermo Fisher Scientific, Tokyo, Japan) at the Support Center for Advanced Medical Sciences, Institute of Biomedical Sciences, Tokushima University Graduate School by Ikuko Sagawa. In brief, protein-containing solutions were reduced with 10 mM DTT/8 M urea and Tris buffer containing 2 mM EDTA (pH 8.5), alkylated with 25 mM iodoacetamide/8 M Urea and Tris buffer containing 2 mM EDTA (pH 8.5), subsequently diluted with trypsin (pig-derived trypsin) and digested overnight at 37°C. Peptides were purified and concentrated by solid-phase extraction (SPE) in ZipTip µC18 pipette tips (Merck Millipore, Darmstadt, Germany). Nano LC-MS/MS was carried out using an UltiMate 3000 RSLC nano system. The reconstituted peptides were injected into an Acclaim PepMap C18 trap column (75 µm × 15 cm, 2 µm, C18) (Merck Millipore, Darmstadt, Germany). Solvent A was 0.1% formic acid. Solvent B was 80% acetonitrile/0.08% formic acid. The peptides were eluted in a 229-min gradient of 4% solvent B in solvent A to 90% solvent B in solvent A at 300 nl/min. Orbitrap Elite's ionization method was set to Nanoflow-LC ESI, positive, and the capillary voltage was set to 1.7 kV. Tandem mass spectrometry was performed using the Proteome Discoverer software program, version 1.4 (Thermo Fisher Scientific, Tokyo, Japan). Charge stated deconvolution and deisotoping were not performed.

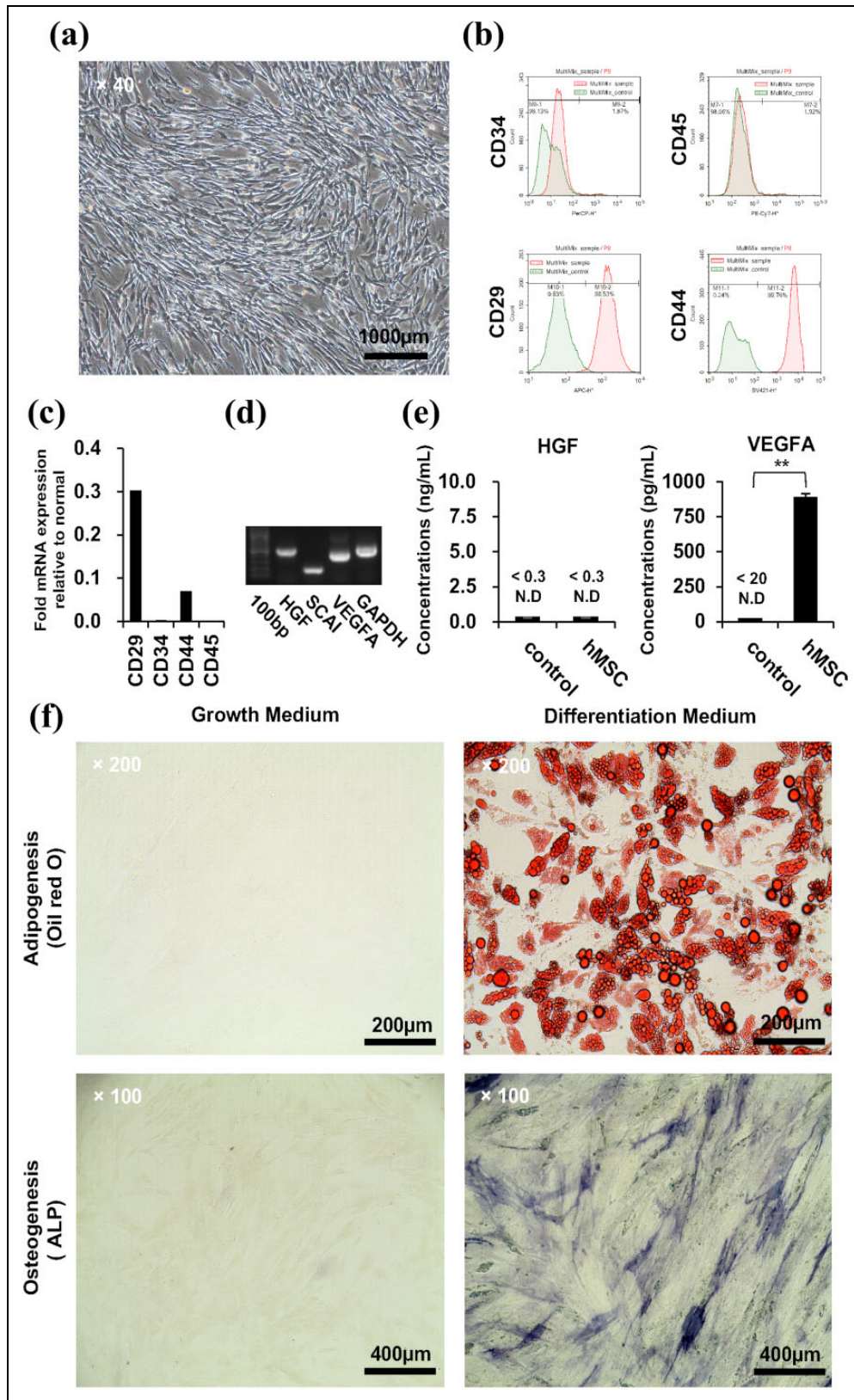


Fig. 2. The phenotype and differentiation potential of hMSC-AT in culture. (a) The morphological appearance of hMSC-AT on day 3. (b) The results of flow cytometry of the cell surface markers of hMSC-AT. (c) The results of real-time PCR to detect cell surface markers of hMSC-AT. The expression was calculated using the $\Delta\Delta\text{Ct}$ method. The expression of the target gene was corrected by the expression of the housekeeping gene. The relative values are indicated. $n = 1$. (d) The results of an RT-PCR to evaluate the growth factor and cell surface markers mRNA expression of hMSC-AT. (e) The results of an ELISA to evaluate the growth factor protein expression of hMSC-AT-CM. (f) Representative images of adipocyte and osteocyte differentiation of hMSC-AT cultured in growth or differentiation medium.

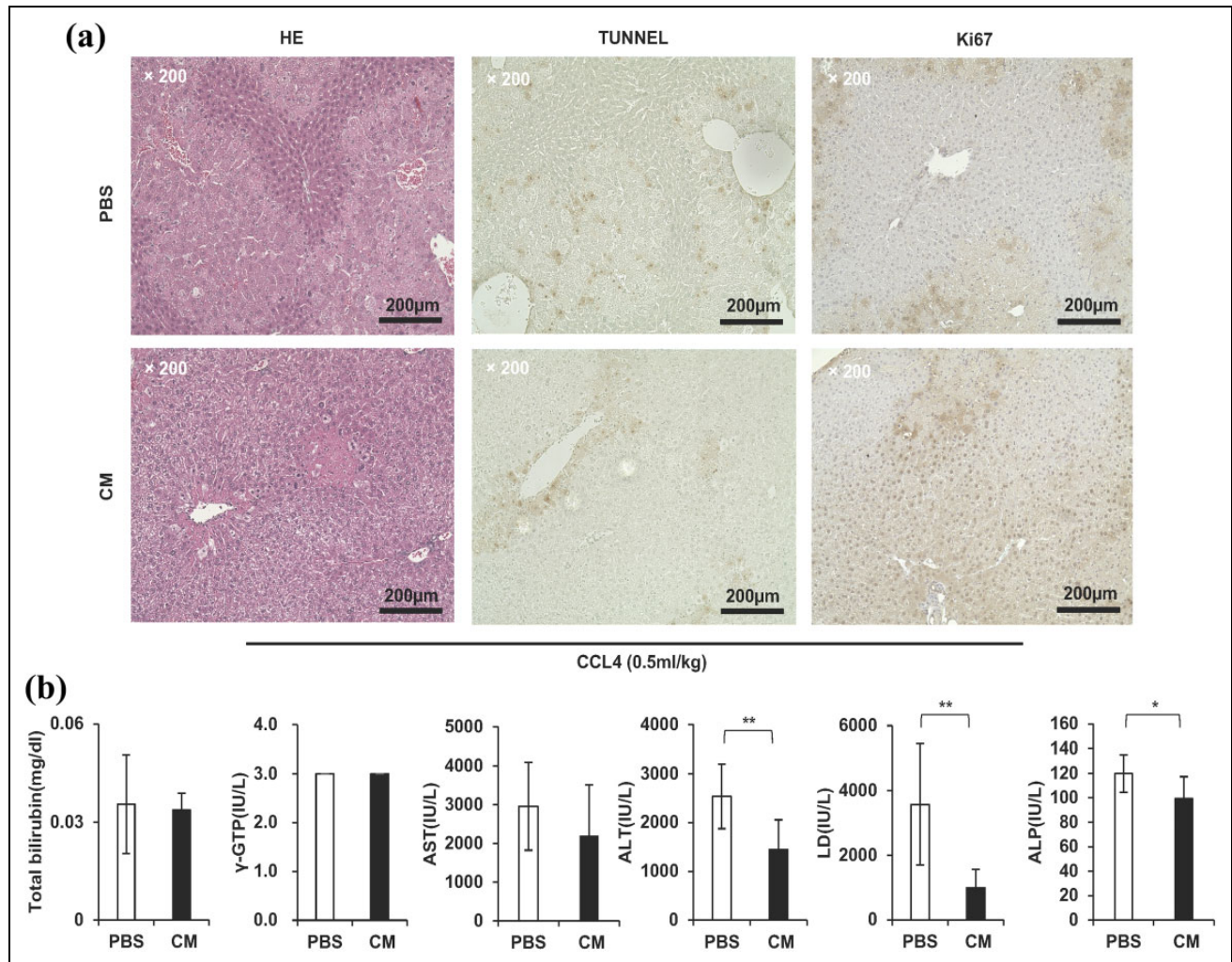


Fig. 3. The culture supernatant concentrate significantly improved the symptoms of acute liver failure caused by the administration of CCL4. (a) Micrographic image of H&E staining (left panel), TUNEL assay (middle panels) and tissue immunostaining of Ki67 (right panel) of liver specimens. Scale bar = 200 μm. (b) In the group to which the culture supernatant concentrate was administered, the total bilirubin (95%), AST (74%), ALT (57%), LD (28%), and ALP (83%) decreased in comparison with the group to which PBS was administered. The decrease in the ALT, LD, and ALP values was significant (** $P < 0.01$, $n = 9$).

Data Analyses

Database Searching

All raw data were searched against the SwissProt 2016-07 database using the Mascot 2.5.1 software program (Matrix Science, London, UK) (unknown version, 551705 entries). The peptide tolerance was set to 10 ppm, and the MS/MS tolerance was set to 0.6 Da. The false discovery rates (FDRs) were calculated for each of the samples using the following formula: $FDR = (N_{decoy}/N_{real} + N_{decoy}) \times 100$. This is an indication of the percentage of the random or “false” peptide identifications in the raw data. The relative abundance of the proteins identified by LC-MS/MS was estimated by determining the protein abundance index (PAI) and the exponentially modified protein abundance index (emPAI). Visualized and validated complex LC-MS/MS proteomics

experiments were performed using Scaffold (version 4.7.3, Proteome Software Inc., Portland, OR, USA – <http://www.proteomesoftware.com/>) to compare samples in order to identify biological relevance.

The Criteria for Protein Identification

The Scaffold software program was used to validate the MS/MS-based peptide and protein identifications. Peptide identifications were accepted if they could be established at > 46.0% probability to achieve an FDR of < 1.0% by the Scaffold Local FDR algorithm. Protein identifications were accepted if they could be established at > 5.0% probability to achieve an FDR of < 1.0% and contained at least 2 identified peptides. Protein probabilities were assigned by the Protein Prophet algorithm¹⁷. Proteins that contained similar peptides

and could not be differentiated based on MS/MS alone were grouped to satisfy the principles of parsimony. Proteins that shared significant peptide evidence were grouped into clusters. A protein GO analysis was performed using the GO analysis function of the Scaffold 4 software program with imported data (goa_uniprot_all.gaf [downloaded 2016/10/14]) from the external GO Annotation Source database.

Results

The Characteristics and Cell Quality of hMSC-ATs

hMSC-ATs were cultured to an 80% confluent state using Clinical Xeno-free medium. We observed the absence of abnormalities in cell size, shape, and culture state with a normal microscope (Fig. 2(a)). Flow cytometry was performed using markers of hMSC-AT (CD 29, CD 44), hematopoietic stem cells (CD 34), and leukocytes (CD 45). Markers of CD29 and CD44 were expressed in hMSC-AT, while the expression of CD34 and CD45 was not detected (Fig. 2(b)). The expression of hMSC-AT markers (CD29, CD44), hematopoietic stem cells (CD34), and leukocytes (CD45) was examined by real-time PCR. CD29 and CD44 were expressed by hMSC-AT, while the expression of CD34 and CD45 was not detected (Fig. 2(c)). The PCR method was used to examine the mRNA expression levels of hepatocyte growth factor (HGF), a suppressor of cancer cell invasion (SCAI) and vascular endothelial growth factor A (VEGFA) expressed in hMSC-AT. (Fig. 2(d)). hMSC-AT-CM was prepared using DMEM/F12 medium. Prior to concentrating hMSC-AT-CM to 1/20 using a 10 k filter, the protein concentration was measured using an ELISA (Fig. 1(a)). The expression of hMSC-AT secreted proteins was examined by an ELISA (R&D Systems, Minneapolis, MN, USA), which revealed that hMSC-AT secreted VEGFA proteins into the culture medium (control group: < 20 [N.D] \pm 0.00 pg/ml, $n = 3$; hMSC group: 886.67 ± 28.93 pg/ml, $n = 3$) (Fig. 2(e)). hMSC-AT have been reported to secrete HGF9. In our experiments, we could not show the measurement because the detection limit of the ELISA (Otuka, Tokyo, Japan) to detect HGF (0.3 ng/ml) was high (control group: < 0.3 [N.D] \pm 0.00 ng/ml, $n = 3$; hMSC group: $< 0.3 \pm 0.00$ ng/ml, $n = 3$). We induced differentiation into adipocytes (Fig. 2(f), upper panels) and osteoblasts (Fig. 2(f), lower panel) using hMSC-AT. Mature adipocytes were stained with Oil Red O and mature osteoblasts were stained with alkaline phosphatase (Fig. 2(f), right panel). hMSC-ATs were cultured in three wells of a six-well plate. Adipocytes stained red with Oil Red O staining in all three wells and osteoblasts stained blue with alkaline phosphatase staining in all three wells were confirmed with a normal microscope.

hMSC-AT-CM Improves the Liver Function of Mice with Acute Liver Failure

CCL4 was intraperitoneally (i.p.) administered to mice to induce hepatic cell damage and model mice were prepared.

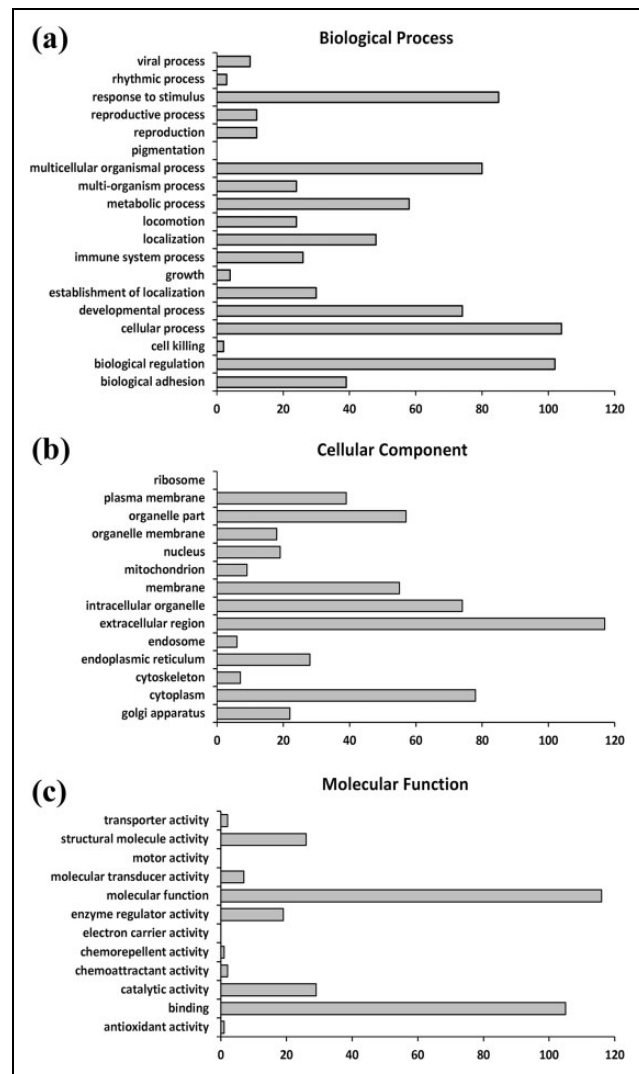


Fig. 4. The biological processes, cellular components and molecular function of the hMSC-AT-CM proteins (as determined by GO). The PCA of proteome dynamics based on the protein information generated by high-resolution mass spectrometry. (a) The ordinate shows each protein's biological function, and the abscissa indicates the proteins that were identified. The names of the proteins classified in Table 3 are listed by their abbreviated names. (b) The ordinate shows the name of each organelle, and the abscissa indicates the number of proteins identified. The names of the proteins classified in Table 4 are listed by their abbreviated names. (c) The ordinate shows each protein's molecular function, and the abscissa indicates the proteins identified. The names of the proteins classified in Table 5 are listed by their abbreviated names.

The upper part of the photo shows the liver histology at 24 h after the administration of CCL4. The hepatocytes of the centrilobular region showed necrotic change. However, when hMSC-AT-CM was injected into the tail vein at 4 h after the administration of CCL4, the number of necrotic cells was reduced. Cells in the growth phase (shown in the panels of Ki67) and apoptotic cells (shown in the panels of the TUNEL assay) of liver tissue sections were detected. In

Table 3. Biological Process.

UniProt/Swiss-PROT ID	Biological adhesion	Biological regulation	Cellular killing	Cellular process	Developmental process	Establishment of localization	Growth process	Immune system process	Localization process	Locomotion process	Metabolic process	Multi-organism process	Multicellular organismal process	Pigmentation process	Reproduction process	Reproductive process	Response to stimulus	Rhythmic process	Viral process
FINC_HUMAN	FINC	FINC	FINC	FINC	FINC	FINC	FINC	FINC	FINC	FINC	FINC		FINC				FINC		
BGH3_HUMAN																			
CO6A1_HUMAN	CO6A1	CO6A1	CO6A1	CO6A1	CO6A1	CO6A1	CO6A1	CO6A1	CO6A1	CO6A1	CO6A1		CO6A1				CO6A1		
CO6A3_HUMAN	CO6A3	CO6A3	CO6A3	CO6A3	CO6A3	CO6A3	CO6A3	CO6A3	CO6A3	CO6A3	CO6A3		CO6A3				CO6A3		
CO1A2_HUMAN	CO1A2	CO1A2	CO1A2	CO1A2	CO1A2	CO1A2	CO1A2	CO1A2	CO1A2	CO1A2	CO1A2		CO1A2				CO1A2		
PAI1_HUMAN	PAI1	PAI1	PAI1	PAI1	PAI1	PAI1	PAI1	PAI1	PAI1	PAI1	PAI1		PAI1				PAI1		PAI1
FSTL1_HUMAN	FSTL1	FSTL1	FSTL1	FSTL1	FSTL1	FSTL1	FSTL1	FSTL1	FSTL1	FSTL1	FSTL1		FSTL1				FSTL1		
POSTN_HUMAN	POSTN	POSTN	POSTN	POSTN	POSTN	POSTN	POSTN	POSTN	POSTN	POSTN	POSTN		POSTN				POSTN		
MMP2_HUMAN	MMP2	MMP2	MMP2	MMP2	MMP2	MMP2	MMP2	MMP2	MMP2	MMP2	MMP2		MMP2				MMP2		
CO1A1_HUMAN	CO1A1	CO1A1	CO1A1	CO1A1	CO1A1	CO1A1	CO1A1	CO1A1	CO1A1	CO1A1	CO1A1		CO1A1				CO1A1		
FBN1_HUMAN	FBN1	FBN1	FBN1	FBN1	FBN1	FBN1	FBN1	FBN1	FBN1	FBN1	FBN1		FBN1				FBN1		
FBN2_HUMAN	FBN2	FBN2	FBN2	FBN2	FBN2	FBN2	FBN2	FBN2	FBN2	FBN2	FBN2		FBN2				FBN2		
CATB_HUMAN	CATB	CATB	CATB	CATB	CATB	CATB	CATB	CATB	CATB	CATB	CATB		CATB				CATB		CATB
LAMB1_HUMAN	LAMB1	LAMB1	LAMB1	LAMB1	LAMB1	LAMB1	LAMB1	LAMB1	LAMB1	LAMB1	LAMB1		LAMB1				LAMB1		
PGS2_HUMAN	PGS2	PGS2	PGS2	PGS2	PGS2	PGS2	PGS2	PGS2	PGS2	PGS2	PGS2		PGS2				PGS2		PGS2
CO6A2_HUMAN	CO6A2	CO6A2	CO6A2	CO6A2	CO6A2	CO6A2	CO6A2	CO6A2	CO6A2	CO6A2	CO6A2		CO6A2				CO6A2		CO6A2
LTBP1_HUMAN	LTBP1	LTBP1	LTBP1	LTBP1	LTBP1	LTBP1	LTBP1	LTBP1	LTBP1	LTBP1	LTBP1		LTBP1				LTBP1		LTBP1
TSP1_HUMAN	TSP1	TSP1	TSP1	TSP1	TSP1	TSP1	TSP1	TSP1	TSP1	TSP1	TSP1		TSP1				TSP1		TSP1
TIMP1_HUMAN	TIMP1	TIMP1	TIMP1	TIMP1	TIMP1	TIMP1	TIMP1	TIMP1	TIMP1	TIMP1	TIMP1		TIMP1				TIMP1		TIMP1
AMRN_HUMAN																			
CO3A1_HUMAN	CO3A1	CO3A1	CO3A1	CO3A1	CO3A1	CO3A1	CO3A1	CO3A1	CO3A1	CO3A1	CO3A1		CO3A1				CO3A1		CO3A1
CFAH_HUMAN	CFAH	CFAH	CFAH	CFAH	CFAH	CFAH	CFAH	CFAH	CFAH	CFAH	CFAH		CFAH				CFAH		CFAH
LTBP2_HUMAN	LTBP2	LTBP2	LTBP2	LTBP2	LTBP2	LTBP2	LTBP2	LTBP2	LTBP2	LTBP2	LTBP2		LTBP2				LTBP2		LTBP2
CO5A1_HUMAN	CO5A1	CO5A1	CO5A1	CO5A1	CO5A1	CO5A1	CO5A1	CO5A1	CO5A1	CO5A1	CO5A1		CO5A1				CO5A1		CO5A1
LG3BP_HUMAN	LG3BP	LG3BP	LG3BP	LG3BP	LG3BP	LG3BP	LG3BP	LG3BP	LG3BP	LG3BP	LG3BP		LG3BP				LG3BP		LG3BP
LAMC1_HUMAN	LAMC1	LAMC1	LAMC1	LAMC1	LAMC1	LAMC1	LAMC1	LAMC1	LAMC1	LAMC1	LAMC1		LAMC1				LAMC1		LAMC1
MFAP2_HUMAN	MFAP2	MFAP2	MFAP2	MFAP2	MFAP2	MFAP2	MFAP2	MFAP2	MFAP2	MFAP2	MFAP2		MFAP2				MFAP2		MFAP2
VIME_HUMAN	VIME	VIME	VIME	VIME	VIME	VIME	VIME	VIME	VIME	VIME	VIME		VIME				VIME		VIME
PCOCI_HUMAN	PCOCI	PCOCI	PCOCI	PCOCI	PCOCI	PCOCI	PCOCI	PCOCI	PCOCI	PCOCI	PCOCI		PCOCI				PCOCI		PCOCI
COBA1_HUMAN	COBA1	COBA1	COBA1	COBA1	COBA1	COBA1	COBA1	COBA1	COBA1	COBA1	COBA1		COBA1				COBA1		COBA1
PEDF_HUMAN	PEDF	PEDF	PEDF	PEDF	PEDF	PEDF	PEDF	PEDF	PEDF	PEDF	PEDF		PEDF				PEDF		PEDF
SPRC_HUMAN	SPRC	SPRC	SPRC	SPRC	SPRC	SPRC	SPRC	SPRC	SPRC	SPRC	SPRC		SPRC				SPRC		SPRC
GAS6_HUMAN	GAS6	GAS6	GAS6	GAS6	GAS6	GAS6	GAS6	GAS6	GAS6	GAS6	GAS6		GAS6				GAS6		GAS6
LEGI_HUMAN	LEGI	LEGI	LEGI	LEGI	LEGI	LEGI	LEGI	LEGI	LEGI	LEGI	LEGI		LEGI				LEGI		LEGI
OLF3_HUMAN	OLF3	OLF3	OLF3	OLF3	OLF3	OLF3	OLF3	OLF3	OLF3	OLF3	OLF3		OLF3				OLF3		OLF3
PTX3_HUMAN	PTX3	PTX3	PTX3	PTX3	PTX3	PTX3	PTX3	PTX3	PTX3	PTX3	PTX3		PTX3				PTX3		PTX3
LAMA2_HUMAN	LAMA2	LAMA2	LAMA2	LAMA2	LAMA2	LAMA2	LAMA2	LAMA2	LAMA2	LAMA2	LAMA2		LAMA2				LAMA2		LAMA2
ITGBL1_HUMAN																			
AEBP1_HUMAN	AEBP1	AEBP1	AEBP1	AEBP1	AEBP1	AEBP1	AEBP1	AEBP1	AEBP1	AEBP1	AEBP1		AEBP1				AEBP1		AEBP1
COS2A2_HUMAN	COS2A2	COS2A2	COS2A2	COS2A2	COS2A2	COS2A2	COS2A2	COS2A2	COS2A2	COS2A2	COS2A2		COS2A2				COS2A2		COS2A2
FBLN1_HUMAN	FBLN1	FBLN1	FBLN1	FBLN1	FBLN1	FBLN1	FBLN1	FBLN1	FBLN1	FBLN1	FBLN1		FBLN1				FBLN1		FBLN1
ENOA_HUMAN	ENOA	ENOA	ENOA	ENOA	ENOA	ENOA	ENOA	ENOA	ENOA	ENOA	ENOA		ENOA				ENOA		ENOA
FBLN5_HUMAN	FBLN5	FBLN5	FBLN5	FBLN5	FBLN5	FBLN5	FBLN5	FBLN5	FBLN5	FBLN5	FBLN5		FBLN5				FBLN5		FBLN5
LUM_HUMAN	LUM	LUM	LUM	LUM	LUM	LUM	LUM	LUM	LUM	LUM	LUM		LUM				LUM		LUM
DKK3_HUMAN	DKK3	DKK3	DKK3	DKK3	DKK3	DKK3	DKK3	DKK3	DKK3	DKK3	DKK3		DKK3				DKK3		DKK3
CO4A2_HUMAN	CO4A2	CO4A2	CO4A2	CO4A2	CO4A2	CO4A2	CO4A2	CO4A2	CO4A2	CO4A2	CO4A2		CO4A2				CO4A2		CO4A2
CSPG2_HUMAN	CSPG2	CSPG2	CSPG2	CSPG2	CSPG2	CSPG2	CSPG2	CSPG2	CSPG2	CSPG2	CSPG2		CSPG2				CSPG2		CSPG2
SRPX_HUMAN	SRPX	SRPX	SRPX	SRPX	SRPX	SRPX	SRPX	SRPX	SRPX	SRPX	SRPX		SRPX				SRPX		SRPX

(continued)

Table 3. (continued)

UniProt/Swiss-Prot ID	Biological adhesion	Biological regulation	Cell killing	Cellular process	Developmental process	Establishment of localization	Growth process	Immune system process	Localization process	Locomotion process	Metabolic process	Multi-organism process	Multicellular organismal process	Pigmentation process	Reproduction process	Reproductive process	Response to stimulus	Rhythmic process	Viral process
CIS_HUMAN	CIS							CIS											
ECM1_HUMAN	ECM1	ECM1	ECM1	ECM1	ECM1			ECM1					ECM1				ECM1		
NIDI_HUMAN	NIDI	NIDI	NIDI	NIDI	NIDI								NIDI						
SAP_HUMAN	SAP	SAP	SAP	SAP	SAP	SAP	SAP	SAP					SAP	SAP	SAP	SAP	SAP		
SEM7A_HUMAN	SEM7A	SEM7A	SEM7A	SEM7A	SEM7A	SEM7A	SEM7A	SEM7A					SEM7A				SEM7A		
CLUS_HUMAN	CLUS	CLUS	CLUS	CLUS	CLUS	CLUS	CLUS	CLUS					CLUS				CLUS		
LYOX_HUMAN	LYOX	LYOX	LYOX	LYOX	LYOX								LYOX				LYOX		
QSOX1_HUMAN	QSOX1	QSOX1	QSOX1	QSOX1	QSOX1	QSOX1	QSOX1	QSOX1					QSOX1						
G3P_HUMAN	G3P	G3P	G3P	G3P	G3P			G3P					G3P				G3P		
TICNI_HUMAN	TICNI	TICNI	TICNI	TICNI	TICNI			TICNI					TICNI				TICNI		
EMILI_HUMAN	EMILI																		
WISP2_HUMAN	WISP2	WISP2	WISP2	WISP2													WISP2		
TFPII_HUMAN	TFPII	TFPII	TFPII	TFPII							TFPII	TFPII	TFPII				TFPII		
PXDN_HUMAN	PXDN	PXDN	PXDN	PXDN				PXDN			TFPII								
PGBM_HUMAN	PGBM	PGBM	PGBM	PGBM							PGBM		PGBM						
IBP4_HUMAN	IBP4	IBP4	IBP4	IBP4				IBP4			PGBM		IBP4				IBP4		
VASN_HUMAN	VASN	VASN	VASN	VASN													VASN		
GNPMB_HUMAN	GNPMB	GNPMB	GNPMB	GNPMB	GNPMB								GNPMB				GNPMB		
SRCL_HUMAN	SRCL	SRCL	SRCL	SRCL	SRCL	SRCL	SRCL	SRCL					SRCL				SRCL		
FBLN3_HUMAN	FBLN3	FBLN3	FBLN3	FBLN3							FBLN3		FBLN3				FBLN3		
PLTP_HUMAN	PLTP	PLTP	PLTP	PLTP	PLTP	PLTP	PLTP	PLTP					PLTP				PLTP		
PROF1_HUMAN	PROF1	PROF1	PROF1	PROF1	PROF1								PROF1				PROF1		
IBP7_HUMAN	IBP7	IBP7	IBP7	IBP7	IBP7								IBP7				IBP7		
PGS1_HUMAN	PGS1	PGS1	PGS1	PGS1									PGS1				PGS1		
NUCB1_HUMAN	NUCB1	NUCB1	NUCB1	NUCB1									PGS1				NUCB1		
CD44_HUMAN	CD44																		
AGRN_HUMAN	AGRN	AGRN	AGRN	AGRN	AGRN			AGRN					AGRN				AGRN		
MFGM_HUMAN	MFGM	MFGM	MFGM	MFGM	MFGM			MFGM					MFGM				MFGM		
RCN1_HUMAN	RCN1	RCN1	RCN1	RCN1	RCN1								RCN1						
FAM3C_HUMAN	FAM3C	FAM3C	FAM3C	FAM3C	FAM3C	FAM3C	FAM3C	FAM3C					FAM3C						
CATZ_HUMAN	CATZ	CATZ	CATZ	CATZ	CATZ	CATZ	CATZ	CATZ					CATZ						
PDIA1_HUMAN	PDIA1	PDIA1	PDIA1	PDIA1									PDIA1				PDIA1		
IBP2_HUMAN	IBP2	IBP2	IBP2	IBP2	IBP2								IBP2				IBP2		
TPPI_HUMAN	TPPI	TPPI	TPPI	TPPI	TPPI								TPPI				TPPI		
GDN_HUMAN	GDN	GDN	GDN	GDN	GDN								GDN				GDN		
CD248_HUMAN	CD248	CD248	CD248	CD248	CD248			CD248					CD248						
SPON2_HUMAN	SPON2	SPON2	SPON2	SPON2	SPON2	SPON2	SPON2	SPON2					SPON2				SPON2		
MARCS_HUMAN	MARCS																		
LAMA1_HUMAN	LAMA1	LAMA1	LAMA1	LAMA1	LAMA1												LAMA1		
SERP_HUMAN	SERP	SERP	SERP	SERP	SERP								SERP				SERP		
PLOD1_HUMAN	PLOD1	PLOD1	PLOD1	PLOD1	PLOD1			PLOD1					PLOD1				PLOD1		
CO4A1_HUMAN	CO4A1																		
GOLM1_HUMAN	GOLM1	GOLM1	GOLM1	GOLM1															
ENPP2_HUMAN	ENPP2	ENPP2	ENPP2	ENPP2	ENPP2	ENPP2	ENPP2	ENPP2					ENPP2				ENPP2		
LAMA4_HUMAN	LAMA4	LAMA4	LAMA4	LAMA4	LAMA4														
TARSH_HUMAN	TARSH	TARSH	TARSH	TARSH	TARSH														
PTK7_HUMAN	PTK7	PTK7	PTK7	PTK7	PTK7	PTK7	PTK7	PTK7					PTK7				PTK7		
SAP3_HUMAN	SAP3	SAP3	SAP3	SAP3	SAP3	SAP3	SAP3	SAP3					PTK7				PTK7		

(continued)

Table 3. (continued)

UniProt/SWISS- PROT ID	Biological Cell adhesion regulation	Cellular process	Developmental of localization	Growth process	Immune system localization	Locomotion process	Metabolic process	Multi-organism process	Multicellular organismal process	Pigmentation reproduction	Reproductive process	Response to stimulus	Rhythmic process	Viral process
CD109_HUMAN	CD109	CD109	CD109	CD109	CD109				CD109					
PAMRL_HUMAN														
KPYM_HUMAN	KPYM	KPYM												
PTGDS_HUMAN	PTGDS	PTGDS	PTGDS	PTGDS	PTGDS	PTGDS	PTGDS							
IBP6_HUMAN	IBP6	IBP6	localization	localization	localization	locomotion	locomotion		organismal	process	stimulus	stimulus	process	process
PROTID	STC2	STC2	STC2	STC2	STC2	STC2	STC2		STC2	STC2	STC2	STC2		
STC2_HUMAN														
FI80A_HUMAN	CFAB				CFAB							CFAB		
CFAB_HUMAN														
CSTNI_HUMAN	CSTNI													
VASI_HUMAN	VASI	VASI	VASI	VASI	VASI							VASI		
FBLN4_HUMAN														
CATLI_HUMAN	CATLI	CATLI			CATLI		CATLI		CATLI			CATLI		
CAB45_HUMAN														
CTHRI_HUMAN	CTHRI	CTHRI	CTHRI	CTHRI	CTHRI	CTHRI			CTHRI			CTHRI		
MFAP5_HUMAN	MFAP5	MFAP5	MFAP5	MFAP5	MFAP5				MFAP5					
CD59_HUMAN	CD59	CD59	CD59	CD59	CD59	CD59			CD59			CD59		
MIF_HUMAN	MIF	MIF	MIF	MIF	MIF	MIF	MIF					MIF		
CXCL5_HUMAN	CXCL5	CXCL5	CXCL5	CXCL5	CXCL5	CXCL5	CXCL5					CXCL5		
ADAM9_HUMAN	ADAM9	ADAM9	ADAM9	ADAM9	ADAM9	ADAM9	ADAM9		ADAM9			ADAM9		
S10AB_HUMAN	S10AB	S10AB	S10AB	S10AB	S10AB	S10AB	S10AB					S10AB		
MAZAI_HUMAN	MAZAI	MAZAI	MAZAI	MAZAI	MAZAI	MAZAI	MAZAI		MAZAI			MAZAI		
CATK_HUMAN	CATK	CATK	CATK	CATK	CATK	CATK	CATK		CATK			CATK		
CAPI_HUMAN	CAPI	CAPI	CAPI	CAPI	CAPI	CAPI	CAPI		CATK			CAPI		
CYTC_HUMAN	CYTC	CYTC	CYTC	CYTC	CYTC	CYTC	CYTC		CYTC			CYTC		CYTC
MXRAB_HUMAN														
CCD80_HUMAN	CCD80	CCD80			CCD80									
FBLN2_HUMAN	FBLN2													
CORIC_HUMAN	CORIC	CORIC	CORIC	CORIC	CORIC	CORIC	CORIC		CORIC			CORIC		
NPC2_HUMAN	NPC2	NPC2	NPC2	NPC2	NPC2	NPC2	NPC2					NPC2		NPC2
KNLI_HUMAN														
CD9_HUMAN														
CD14_HUMAN														

mouse liver administered hMSC-AT-CM, the number of apoptotic cells widely observed in liver tissues was reduced by CCL4 administration. Furthermore, the apoptotic cells were localized to the interlobular vein in liver tissues treated with hMSC-AT-CM. Cells in the growth phase were observed around the cells showing apoptosis due to the administration of CCL4 (Fig. 3(a), left and middle panels). However, cells in the growth phase were uniformly observed in liver tissues treated with hMSC-AT-CM. Ki67 was expressed only in the nucleus, and cells in the proliferation phase had brown-stained nuclei. Mouse hepatocytes in the group treated with hMSC-AT-CM showed more nuclear-stained cells than those in the group treated with PBS, thus indicating that hMSC-AT-CM promoted hepatocyte proliferation (Fig. 3(a), right panel). We also counted the number of positively stained cells in images of TUNNEL-stained sections ($\times 100$). The numbers of positively stained cells in the PBS and CM groups were 15.25 ± 3.96 and 10.00 ± 5.07 , respectively ($n = 4$; $P = 0.18$) (Fig. 3(a), middle panels). We also counted the number of cells with positively stained nuclei on images of Ki67-stained sections ($\times 100$). The numbers of cells with positively stained nuclei in the PBS and CM groups were 10.25 ± 4.23 and 90.75 ± 38.42 , respectively ($n = 4$; $** P < 0.01$) (Fig. 3(a), right panels). These results indicate that hMSC-AT-CM rapidly recovered because of the generation of new viable cells as the older cells died due to CCL4 administration (Fig. 3(a)).

Our experiments show that the administration of MSC-AT-CM from a single vein rapidly promoted the cellular proliferation of mouse hepatocytes. The proteins associated with a growth function (GO analysis), identified by the presence of MSC-AT-CM, were POSTN, SAP, SEM7A, PTK7 (Table 3). Of course, it is not possible to explain the proliferative effect of hepatocytes based on the presence of four proteins. Periostin, which is encoded by the POSTN gene, has been reported as an extracellular factor that promotes hepatosteatosis^{18,19}; however, many points about proteins with the ability to promote the cellular proliferation of hepatocytes remain unclear. P component (SAP) is a protein that is expressed in hepatocytes and secreted into serum, and is known to be involved in processes associated with immune regulation, such as the action of opsonins²⁰. Whether SAP is involved in the cellular proliferation of hepatocytes is unknown. Semaphorin 7A (SEM7A) is known to contribute to TGF- β mediated hepatic fibrosis²¹. It is unknown whether SEM7A promotes hepatocyte cell proliferation. Thus, future studies should investigate whether the growth-associated proteins that are newly identified by GO analyses promote the cellular proliferation of hepatocytes with CCL4-induced impairment. At approximately 10 days of gestation, during the development of the liver, the hematopoietic cells flow from the aorta-gonad-mesonephros region (AGM region) and placenta, and the liver begins to function as a hematopoietic organ²². It has been clarified that HGF and various extracellular matrices produced by non-parenchymal cells promote the differentiation of hepatoblasts into hepatocytes

during this period²³. In addition, a recent theory suggests that the biliary tree functions as a source of liver and pancreatic stem cells and progenitor cells. It is known that VEGF is secreted by the biliary tree due as a stress response²⁴. From these developmental perspectives, it can be hypothesized that the HGF and VEGF secreted by MSC-AT-CMs have an extremely strong promoting effect on hepatocyte proliferation.

Serum from the model mice was sampled and biochemically analyzed. The average value of each measurement was as follows (correction was not made by diluting 100 μ L of serum with 400 μ L of physiological saline). Total bilirubin (PBS 0.04 ± 0.02 , supernatant concentrate 0.03 ± 0.01 (unit mg/ml)), AST (PBS 2956 ± 1133 , supernatant concentrate 2195 ± 1319 (unit IU/L)), ALT (PBS 2538 ± 663 , supernatant concentrate 1448 ± 608 (unit IU/L)), LD (PBS 3574 ± 1873 , supernatant concentrate 997 ± 572 (unit IU/L)), ALP (PBS 120 ± 15 , supernatant concentrate 99 ± 18 (unit IU/L)). The serum liver injury markers (ALT, LD and ALP) were significantly reduced at 20 h after the administration of hMSC-AT-CM (Fig. 3(b)).

The Biological Processes, Cellular Components and Molecular Function of Proteins Identified from hMSC-AT-CM

The biological processes of proteins were analyzed using the Mascot software program with the SwissProt 2016 database.

In this study, a secreted protein expression analysis of hMSC-AT was performed using LC-MS/MS and 128 proteins were identified (Table 1). LC-MS/MS showed that 106 new functional proteins and 22 proteins (FINC, PAI1, POSTN, PGS2, TIMP1, AMPN, CFAH, VIME, PEDF, SPRC, LEG1, ITGBL, ENOA, CSPG2, CLUS, IBP4, IBP7, PGS1, IBP2, STC2, CTHR1, CD9) were previously reported in hMSC-AT-CMs. In addition, various proteins associated with growth (SAP, SEM7A, PTK7); immune system processes (CO1A2, CO1A1, CATB, TSP1, GAS6, PTX3, C1 S, SEM7A, G3P, PXDN, SRCRL, CD248, SPON2, ENPP2, CD109, CFAB, CATL1, MFAP5, MIF, CXCL5, ADAM9, CATK); and reproduction (MMP2, CATB, FBLN1, SAP, MFGM, GDN, CYTC) were identified in hMSC-AT-CMs.

Biological processes. FINC, CATB, TSP1, GAS6, SAP, SEM7A, SRCRL, MFGM, GDN, SPON2, PTK7, ADAM9 and CYTC all seemed to be widely involved in the function of hMSC-AT-CM under the classification of 'biological processes' (Table 3). FINC was distributed in sites such as those associated with the response to biological adhesion, biological regulation, cellular processes, the developmental process, the establishment of localization, the immune system process, localization, locomotion, the metabolic process, the multicellular organismal process, and response to stimulus. Collagen types I, V, VI and XII, and fibronectin (ECM components) were detected in hMSC-AT-CM by MALDI-

Table 4. Cellular Component.

UniProt/SWISS-PROT ID	golgi apparatus	cytoplasm	cytoskeleton	endoplasmic reticulum	endosome	extracellular region	intracellular organelle	membrane	mitochondrion	nucleus	organelle membrane	organelle part	plasma membrane	ribosome
FINC_HUMAN		FINC				FINC	FINC	FINC				FINC	FINC	
BGH3_HUMAN	BGH3	BGH3				BGH3	BGH3	BGH3				BGH3	BGH3	
CO6A1_HUMAN		CO6A1		CO6A1		CO6A1	CO6A1	CO6A1			CO6A1	CO6A1	CO6A1	
CO6A3_HUMAN		CO6A3		CO6A3		CO6A3	CO6A3	CO6A3				CO6A3	CO6A3	
CO1A2_HUMAN		CO1A2		CO1A2		CO1A2	CO1A2					CO1A2	CO1A2	
PAII_HUMAN		PAII				PAII	PAII	PAII				PAII	PAII	
FSTL1_HUMAN						FSTL1								
POSTN_HUMAN	POSTN	POSTN				POSTN	POSTN					POSTN		
MMP2_HUMAN		MMP2				MMP2	MMP2	MMP2	MMP2	MMP2		MMP2	MMP2	
CO1A1_HUMAN	CO1A1	CO1A1		CO1A1		CO1A1	CO1A1					CO1A1		
FBN1_HUMAN						FBN1								
FBN2_HUMAN						FBN2								
CATB_HUMAN		CATB		CATB		CATB	CATB		CATB	CATB		CATB		
LAMBI_HUMAN		LAMBI				LAMBI								
PGS2_HUMAN	PGS2	PGS2				PGS2	PGS2					PGS2		
CO6A2_HUMAN		CO6A2		CO6A2		CO6A2	CO6A2	CO6A2				CO6A2	CO6A2	
LTBP1_HUMAN						LTBP1								
TSP1_HUMAN		TSP1		TSP1		TSP1	TSP1	TSP1				TSP1	TSP1	
TIMP1_HUMAN		TIMP1				TIMP1	TIMP1					TIMP1		
AMPN_HUMAN		AMPN				AMPN	AMPN	AMPN			AMPN	AMPN	AMPN	
CO3A1_HUMAN		CO3A1		CO3A1		CO3A1	CO3A1					CO3A1		
CFAH_HUMAN						CFAH								
LTBP2_HUMAN						LTBP2								
CO5A1_HUMAN		CO5A1		CO5A1		CO5A1	CO5A1					CO5A1		
LG3BP_HUMAN		LG3BP				LG3BP	LG3BP	LG3BP				LG3BP		
LAMC1_HUMAN						LAMC1								
MFAP2_HUMAN						MFAP2								
VIME_HUMAN		VIME	VIME			VIME	VIME	VIME				VIME	VIME	
PCOCI_HUMAN						PCOCI								
COBA1_HUMAN		COBA1		COBA1		COBA1	COBA1					COBA1		
PEDF_HUMAN		PEDF				PEDF	PEDF							
SPRC_HUMAN		SPRC				SPRC	SPRC	SPRC	SPRC	SPRC	SPRC	SPRC	SPRC	
GAS6_HUMAN	GAS6	GAS6		GAS6		GAS6	GAS6					GAS6		
LEGI_HUMAN		LEGI				LEGI	LEGI			LEGI				
OLF3_HUMAN						OLF3								
PTX3_HUMAN						PTX3								
LAMA2_HUMAN						LAMA2		LAMA2					LAMA2	
ITGBL_HUMAN						ITGBL								
AEBP1_HUMAN		AEBP1				AEBP1	AEBP1							
CO5A2_HUMAN		CO5A2		CO5A2		CO5A2	CO5A2					CO5A2		
FBLN1_HUMAN		ENOA				FBLN1	ENOA					ENOA	ENOA	
ENOA_HUMAN		ENOA				ENOA	ENOA	ENOA		ENOA		ENOA	ENOA	
FBLN5_HUMAN		LUM				FBLN5	LUM					LUM		
LUM_HUMAN	LUM	LUM				LUM	LUM					LUM		
DKK3_HUMAN						DKK3								
CO4A2_HUMAN		CO4A2		CO4A2		CO4A2	CO4A2					CO4A2		

(continued)

Table 4. (continued)

UniProt/SWISS-PROT ID	golgi apparatus	cytoplasm	cytoskeleton	endoplasmic reticulum	endosome	extracellular region	intracellular organelle	membrane	mitochondrion	nucleus	organelle membrane	organelle part	plasma membrane	ribosome
CSPG2_HUMAN	CSPG2	CSPG2				CSPG2	CSPG2	CSPG2				CSPG2		
SRPX_HUMAN		SRPX		SRPX			SRPX	SRPX						
C1S_HUMAN						C1S								
ECM1_HUMAN		ECM1				ECM1	ECM1					ECM1		
NIDI_HUMAN						NIDI								
SAP_HUMAN		SAP				SAP	SAP	SAP	SAP		SAP			
SEM7A_HUMAN						SEM7A		SEM7A					SEM7A	
CLUS_HUMAN		CLUS		CLUS		CLUS	CLUS	CLUS	CLUS	CLUS	CLUS	CLUS		
LYOX_HUMAN						LYOX	LYOX			LYOX				
QSOX1_HUMAN	QSOX1	QSOX1				QSOX1	QSOX1	QSOX1		QSOX1	QSOX1	QSOX1		
G3P_HUMAN		G3P	G3P			G3P	G3P	G3P		G3P	G3P	G3P	G3P	
TICN1_HUMAN		TICN1				TICN1								
EMIL1_HUMAN						EMIL1								
WISP2_HUMAN						WISP2								
TFPI1_HUMAN		TFPI1		TFPI1		TFPI1	TFPI1	TFPI1	TFPI1	TFPI1	TFPI1	TFPI1	TFPI1	
PXDN_HUMAN		PXDN		PXDN		PXDN	PXDN							
PGBM_HUMAN	PGBM	PGBM				PGBM	PGBM	PGBM			PGBM	PGBM	PGBM	
IBP4_HUMAN						IBP4								
VASN_HUMAN		VASN				VASN	VASN	VASN	VASN		VASN	VASN	VASN	
GNPMB_HUMAN		GNPMB				GNPMB	GNPMB	GNPMB					GNPMB	
SRCL_HUMAN		SRCL				SRCL	SRCL	SRCL						
FBLN3_HUMAN						FBLN3								
PLTP_HUMAN						PLTP								
PROFI_HUMAN		PROFI	PROFI			PROFI	PROFI	PROFI		PROFI				
IBP7_HUMAN						IBP7								
PGS1_HUMAN	PGS1	PGS1				PGS1	PGS1	PGS1				PGS1	PGS1	
NUCB1_HUMAN	NUCB1	NUCB1	NUCB1	NUCB1	NUCB1	NUCB1	NUCB1	NUCB1	NUCB1	NUCB1	NUCB1	NUCB1	NUCB1	
CD44_HUMAN						CD44		CD44					CD44	
AGRN_HUMAN	AGRN	AGRN				AGRN	AGRN	AGRN			AGRN	AGRN	AGRN	AGRN
MFGM_HUMAN						MFGM		MFGM					MFGM	
RCNI_HUMAN		RCNI		RCNI		RCNI	RCNI					RCNI		
FAM3C_HUMAN	FAM3C	FAM3C				FAM3C	FAM3C					FAM3C		
CATZ_HUMAN	CATZ	CATZ		CATZ		CATZ	CATZ	CATZ			CATZ	CATZ	CATZ	
PDIA1_HUMAN		PDIA1		PDIA1		PDIA1	PDIA1	PDIA1			PDIA1	PDIA1	PDIA1	
IBP2_HUMAN						IBP2	IBP2	IBP2					IBP2	
TPPI_HUMAN		TPPI				TPPI	TPPI		TPPI			TPPI		
GDN_HUMAN		GDN				GDN	GDN	GDN					GDN	
CD248_HUMAN		CD248				CD248		CD248						
SPON2_HUMAN						SPON2								
MARCS_HUMAN		MARCS	MARCS			MARCS	MARCS	MARCS		MARCS		MARCS	MARCS	
LAMA1_HUMAN						LAMA1								
SERPH_HUMAN		SERPH		SERPH		SERPH	SERPH	SERPH				SERPH	SERPH	
PLOD1_HUMAN		PLOD1		PLOD1		PLOD1	PLOD1	PLOD1			PLOD1	PLOD1	PLOD1	
CO4A1_HUMAN						CO4A1								
GOLM1_HUMAN	GOLM1	GOLM1				GOLM1	GOLM1	GOLM1					GOLM1	GOLM1
ENPP2_HUMAN						ENPP2	ENPP2	ENPP2					ENPP2	ENPP2

(continued)

Table 4. (continued)

UniProt/SWISS-PROT ID	golgi apparatus	cytoplasm	cytoskeleton	endoplasmic reticulum	endosome	extracellular region	intracellular organelle	membrane	mitochondrion	nucleus	organelle membrane	organelle part	plasma membrane	ribosome
LAMA4_HUMAN						LAMA4								
TARSH_HUMAN						TARSH								
PTK7_HUMAN								PTK7					PTK7	
SAP3_HUMAN		SAP3				SAP3	SAP3	SAP3	SAP3			SAP3	SAP3	
CD109_HUMAN						CD109		CD109					SAP3	CD109
PAMRI_HUMAN						PAMRI								
KPYM_HUMAN		KPYM				KPYM	KPYM	KPYM	KPYM	KPYM			KPYM	
PTGDS_HUMAN	PTGDS	PTGDS		PTGDS		PTGDS	PTGDS	PTGDS	PTGDS	PTGDS	PTGDS	PTGDS		
IBP6_HUMAN	IBP6	IBP6				IBP6	IBP6							
STC2_HUMAN	STC2	STC2		STC2		STC2	STC2							
FI80A_HUMAN						FI80A								
CFAB_HUMAN						CFAB								
CSTNI_HUMAN	CSTNI	CSTNI		CSTNI		CSTNI	CSTNI	CSTNI	CSTNI	CSTNI	CSTNI	CSTNI	CSTNI	
VASI_HUMAN		VASI			VASI	VASI	VASI	VASI				VASI		
FBLN4_HUMAN						FBLN4								
CATLI_HUMAN					CATLI	CATLI	CATLI					CATLI		
CAB45_HUMAN														
CTHRI_HUMAN						CTHRI								
MFAP5_HUMAN						MFAP5								
CD59_HUMAN	CD59	CD59		CD59		CD59	CD59	CD59		MIF		CD59	CD59	
MIF_HUMAN		MIF				MIF	MIF					MIF		
CXCL5_HUMAN						CXCL5								
ADAM9_HUMAN						ADAM9		ADAM9					ADAM9	
S10AB_HUMAN		S10AB				S10AB	S10AB							
MA2A1_HUMAN	MA2A1	MA2A1				MA2A1	MA2A1	MA2A1		S10AB		MA2A1	MA2A1	
CATK_HUMAN		CATK			CATK	CATK	CATK	MA2A1				CATK	CATK	
CAPI_HUMAN		CAPI	CAPI			CAPI	CAPI	CAPI				CAPI	CAPI	
CYTC_HUMAN		CYTC		CYTC		CYTC	CYTC	CYTC		CYTC		CYTC	CYTC	
MXRA8_HUMAN														
CCD80_HUMAN						CCD80								
FBLN2_HUMAN						FBLN2								
CORIC_HUMAN		CORIC	CORIC				CORIC							CORIC
NPC2_HUMAN		NPC2		NPC2		NPC2	CORIC							
KNLI_HUMAN														
CD9_HUMAN														
CD14_HUMAN														

Table 5. Molecular Function.

UniProt/SWISS-PROT ID	Antioxidant activity	Binding	Catalytic activity	Chemoattractant activity	Chemorepellent activity	Electron carrier activity	Enzyme regulator activity	Molecular function	Molecular transducer activity	Motor activity	Structural molecule activity	Transporter activity
FINC_HUMAN		FINC					FINC	FINC				
BGH3_HUMAN		BGH3						BGH3				
CO6A1_HUMAN		CO6A1						CO6A1				
CO6A3_HUMAN							CO6A3	CO6A3				
CO1A2_HUMAN		CO1A2						CO1A2			CO1A2	
PAI1_HUMAN		PAI1					PAI1	PAI1				
FSTL1_HUMAN		FSTL1						FSTL1				
POSTN_HUMAN		POSTN						POSTN				
MMP2_HUMAN		MMP2	MMP2					MMP2				
CO1A1_HUMAN		CO1A1						CO1A1			CO1A1	
FBN1_HUMAN		FBN1						FBN1			FBN1	
FBN2_HUMAN		FBN2						FBN2			FBN2	
CATB_HUMAN		CATB	CATB					CATB				
LAMB1_HUMAN								LAMB1			LAMB1	
PGS2_HUMAN		PGS2					PGS2	PGS2				
CO6A2_HUMAN												
LTPB1_HUMAN		LTPB1	LTPB1					LTPB1	LTPB1			
TSPI_HUMAN		TSPI						TSPI				
TIMPI_HUMAN		TIMPI					TIMPI					
AMPN_HUMAN		AMPN	AMPN					AMPN	AMPN			
CO3A1_HUMAN		CO3A1						CO3A1			CO3A1	
CFAH_HUMAN		CFAH						CFAH				
LTPB2_HUMAN		LTPB2						LTPB2				
CO5A1_HUMAN		CO5A1						CO5A1			CO5A1	
LG3BP_HUMAN								LG3BP	LG3BP			
LAMCI_HUMAN								LAMCI			LAMCI	
MFAP2_HUMAN												
VIME_HUMAN		VIME						VIME			VIME	
PCOCI_HUMAN		PCOCI					PCOCI	PCOCI				
COBA1_HUMAN		COBA1						COBA1			COBA1	
PEDF_HUMAN		PEDF					PEDF	PEDF				
SPRC_HUMAN		SPRC						SPRC				
GAS6_HUMAN		GAS6					GAS6	GAS6				GAS6
LEGI_HUMAN		LEGI						LEGI				
OLF3_HUMAN												
PTX3_HUMAN		PTX3						PTX3				
LAMA2_HUMAN		LAMA2						LAMA2			LAMA2	
ITGBL_HUMAN												
AEBP1_HUMAN		AEBP1	AEBP1					AEBP1				
CO5A2_HUMAN		CO5A2						CO5A2			CO5A2	
FBLN1_HUMAN		FBLN1					FBLN1	FBLN1			FBLN1	
ENOA_HUMAN		ENOA	ENOA				ENOA	ENOA				

(continued)

Table 5. (continued)

UniProt/SWISS-PROT ID	Antioxidant activity	Binding	Catalytic activity	Chemoattractant activity	Chemorepellent activity	Electron carrier activity	Enzyme regulator activity	Molecular function	Molecular transducer activity	Motor activity	Structural molecule activity	Transporter activity
FBLN5_HUMAN		FBLN5						FBLN5			LUM	
LUM_HUMAN		LUM						LUM				
DKK3_HUMAN												
CO4A2_HUMAN								CO4A2			CO4A2	
CSPG2_HUMAN		CSPG2						CSPG2			CSPG2	
SRPX_HUMAN												
C1S_HUMAN		C1S	C1S					C1S				
ECM1_HUMAN		ECM1						ECM1				
NIDI_HUMAN		NIDI						NIDI				
SAP_HUMAN		SAP					SAP	SAP				
SEM7A_HUMAN		SEM7A			SEM7A			SEM7A				
CLUS_HUMAN		CLUS	CLUS					CLUS				
LYOX_HUMAN		LYOX	LYOX					LYOX				
QSOX1_HUMAN			QSOX1					QSOX1				
G3P_HUMAN		G3P	G3P					G3P				
TICN1_HUMAN		TICN1						TICN1				
EMIL1_HUMAN		EMIL1						EMIL1			EMIL1	
WISP2_HUMAN		WISP2						WISP2				
TFPII_HUMAN								TFPII				
PXDN_HUMAN	PXDN	PXDN	PXDN					PXDN			PXDN	
PGBM_HUMAN		PGBM						PGBM				
IBP4_HUMAN		IBP4						IBP4				
VASN_HUMAN		VASN						VASN				
GPNMB_HUMAN		GPNMB		GPNMB				GPNMB				
SRCL_HUMAN		SRCL						SRCL	SRCL			
FBLN3_HUMAN		FBLN3	FBLN3					FBLN3	FBLN3			
PLTP_HUMAN		PLTP						PLTP				
PROFI_HUMAN		PROFI						PROFI	PROFI			
IBP7_HUMAN		IBP7						IBP7				
PGS1_HUMAN		PGS1						PGS1	PGS1		PGS1	
NUCBI_HUMAN		NUCBI						NUCBI				
CD44_HUMAN		CD44						CD44				
AGRN_HUMAN		AGRN						AGRN			AGRN	
MFGM_HUMAN		MFGM						MFGM				
RCN1_HUMAN		RCN1						RCN1				
FAM3C_HUMAN		FAM3C						FAM3C				
CATZ_HUMAN		CATZ	CATZ					CATZ				
PDIA1_HUMAN		PDIA1	PDIA1					PDIA1				
IBP2_HUMAN		IBP2						IBP2				
TPPI_HUMAN		TPPI	TPPI					TPPI				
GDN_HUMAN		GDN					GDN	GDN				
CD248_HUMAN		CD248						CD248				
SPON2_HUMAN		SPON2						SPON2				

(continued)

Table 5. (continued)

UniProt/SWISS-PROT ID	Antioxidant activity	Binding	Catalytic activity	Chemoattractant activity	Chemorepellent activity	Electron carrier activity	Enzyme regulator activity	Molecular function	Molecular transducer activity	Motor activity	Structural molecule activity	Transporter activity
MARCS_HUMAN		MARCS						MARCS				
LAMAI_HUMAN		LAMAI						LAMAI			LAMAI	
SERPH_HUMAN		SERPH					SERPH	SERPH				
PLODI_HUMAN		PLODI	PLODI									
CO4A1_HUMAN								CO4A1			CO4A1	
GOLM1_HUMAN		GOLM1						GOLM1				
ENPP2_HUMAN		ENPP2	ENPP2					ENPP2	ENPP2		LAMA4	
LAMA4_HUMAN		LAMA4						LAMA4				
TARSH_HUMAN		TARSH						TARSH				
PTK7_HUMAN		PTK7	PTK7					PTK7	PTK7			
SAP3_HUMAN			SAP3				SAP3	SAP3				SAP3
CD109_HUMAN		CD109					CD109	CD109				
PAMR1_HUMAN		PAMR1						PAMR1				
KPYM_HUMAN		KPYM	KPYM					KPYM				
PTGDS_HUMAN		PTGDS	PTGDS					PTGDS				
IBP6_HUMAN		IBP6						IBP6				
STC2_HUMAN		STC2						STC2				
FI80A_HUMAN												
CFAB_HUMAN			CFAB					CFAB				
CSTNI_HUMAN		CSTNI						CSTNI				
VASI_HUMAN		VASI	VASI					VASI				
FBLN4_HUMAN		FBLN4						FBLN4			FBLN4	
CATLI_HUMAN		CATLI	CATLI					CATLI				
CAB45_HUMAN												
CTHRI_HUMAN		CTHRI						CTHRI				
MFAP5_HUMAN								MFAP5			MFAP5	
CD59_HUMAN		CD59						CD59				
MIF_HUMAN		MIF	MIF	MIF				MIF				
CXCL5_HUMAN		CXCL5						CXCL5				
ADAM9_HUMAN		ADAM9	ADAM9					ADAM9				
S10AB_HUMAN		S10AB						S10AB				
MA2A1_HUMAN		MA2A1	MA2A1					MA2A1				
CATK_HUMAN		CATK	CATK					CATK				
CAPI_HUMAN		CAPI						CAPI				
CYTC_HUMAN		CYTC					CYTC	CYTC				
MXRA8_HUMAN												
CCD80_HUMAN		CCD80						CCD80				
FBLN2_HUMAN		FBLN2						FBLN2			FBLN2	
COR1C_HUMAN		COR1C						COR1C				
NPC2_HUMAN		NPC2						NPC2				
KNL1_HUMAN												
CD9_HUMAN												
CD14_HUMAN												

Table 6. (continued)

Proteins excluded from protein list of hMSC-AT-CM (overlapped with basal medium)	PLoS ONE 2007;issue 9:e941 ¹¹	PLoS ONE 2008;3:e1886	The Journal of Neuroscience 2015;11:2452-2464	Exp Cell Res 2010;16: 1271-1281	STEM CELLS 2008;26:2705-2712 ⁸	TISSUE ENGINEERING 2012;Part A 18:1479-1489 ⁹	Molecular Therapy 2015;23: 549-560	Scientific Reports 2013;4:3652
hMSC-AT ³ -CM ^d	hMSC-BM ¹ -BM ² -CM	hMSC-BM ¹ -CM ⁴¹	hMSC-BM & hMSC-DP ^c -CM ⁴²	hMSC-BM-CM ²⁵	hMSC-BM-CM AT-CM	hMSC-BM-CM	hMSC-BM-CM ⁴³	hMSC-BM-CM ⁴⁴
AEBP1	CCL8	IBP1	ELAF					
CO5A2	CSF1	IBP3	GDF15					
FBLN1	ANG1	IBP4	IL19					
ENO4	EGF	CXCL10	BGH3					
FBLN5	CCL16	LIF	IL5RA					
LUM	AMPL1	TNFI4	SIGL9					
DKK3	CCL5	CCL20	BCAM					
CO4A2	ANGP	CXCL7	HGF					
CSPG2	GROA	NTF3	XCLI					
SRPX	TIMP4	NTF4	VEGFC					
C1S	IBP6	CCL18	TRI1B					
ECM1	TIMP1	PLGF	TIMP2					
NIDI	INHBA	TGFB2	MIF					
SAP	LIF	TGFB3	CD166					
SEM7A	CCL11	TIMP1	HAYRI					
CLUS	HGF	TIMP2	CCL28					
LYOX	CXL10		TNR8					
QSOX1	CCL26		CCL2					
G3P	PDGFA		TPO					
TICN1	BMP7		IL6RA					
EMILI	MMP9		SAA					
WISP2	PDGFB		SCR2					
TFPI1	IGF1		MMP8					
PXDN	MMP1		EPOR					
PGBM	BMP5		PIGF					
IBP4	ADIPO		IL6RA/B					
VASN	IL1RA		TIMP1					
GNPMB	CXCL5		VEGFA					
SRCL	CCL1		IFNL2					
FBLN3	VEGFA		TRI0C					
PLTP	FGF7							

^ahuman Mesenchymal Stem Cells from adipose tissue; ^bhuman Mesenchymal Stem Cells from Bone marrow; ^chuman Mesenchymal Stem Cells from dental pulp; ^dconditional medium.

TOF/TOF mass spectrometry²⁵. Fibronectin is a major ECM component that supports cell adhesion by presenting an integrin binding domain²⁶. FINC in plasma is taken up by the fibrin clot during tissue injury, contributing to the platelet function and hemostasis. The cell's FINC is then synthesized by the cells to reconstitute the damaged tissue²⁷. CATB, TSP1, GAS6, SAP, SEM7A, SRCRL, MFGM, GDN, SPON2, PTK7, ADAM9 and CYTC were newly detected in hMSC-AT-CM. MFGM was distributed in sites such as those associated with the response to biological adhesion, biological regulation, cellular processes, the developmental process, the establishment of localization, localization, the metabolic process, multi-organism processes, multicellular organismal processes, reproduction, the reproductive process, and the viral process. Jang et al. presented a pathology model showing that MFGM inhibits hepatic fibrosis via the signal of transforming growth factor (TGF)- β ²⁸ (Fig. 4a).

Cellular components. Proteins synthesized in the rough endoplasmic reticulum are transported to the lumen of the rough endoplasmic reticulum and transported or secreted to the cell membrane via the Golgi apparatus. In hMSC-AT-CM, GAS6, CLUS, NUCB1, CATZ, PTGDS, STC2, CSTN1, and CD59 also seem to be widely involved in the function of hMSC-AT-CM under the classifications of endoplasmic reticulum, Golgi apparatus, membrane, and extracellular region of 'cellular component' (Table 4). STC2 suppresses the oxidative stress-induced cell damage of MSC. In the clinical application of MSC, it was suggested that STC2 promotes the long-term therapeutic effects of therapeutic cells²⁹. GAS6, CLUS, NUCB1, CATZ, CSTN1 and CD59 were newly detected in hMSC-AT-CM (Fig. 4b).

Molecular function. In hMSC-AT-CM, LTBP1, AMPN, GAS6, FBLN1, PXDN, FBLN3, PGS1, ENPP2, PTK7 and MIF also seem to be widely involved in the function of hMSC-AT-CM under the classification of 'molecular function' (Table 5).

POSTN, PGS2, TIMP1, PEDF, LEG1 and IBP7, the protein function of which was not especially wide was related to the biological processes, cellular components and molecular function of hMSCs (Table 1). POSTN has previously been reported as a factor that promotes the *in vivo* proliferation activity of cancer in association with hACS transplantation³⁰. POSTN has been reported to promote the cell migration of MSC-BM via PI3K/Akt signaling through receptor integrin α v β 3³¹. The simultaneous administration of MSC-BM and PGS2 was reported to significantly improve thioacetamide-induced the rat model of hepatic fibrosis in comparison with the administration of MSC-BM alone³². The TIMP1 contained in the culture supernatant of the immortalized MSC line RCB2157 was reported to inhibit the migration and invasion of breast cancer cells³³. MSC-BM in aged mice show the increased expression of PEDF. PEDF was reported to promote or inhibit the growth of cells

affected by myocardial infarction³⁴. PEDF has also been reported to promote the expression of bone formation genes and mineral deposition genes of human MSC-BM³⁵. It has been reported that IBP7 has an important function in the action of MSC-BM in preparation for immune regulation in a mouse model of colitis³⁶. LTBP1, AMPN, GAS6, FBLN1, PXDN, FBLN3, PGS1, ENPP2, PTK7 and MIF were newly detected in hMSC-AT-CM (Fig. 4c).

Discussion

In recent years, genome sequencing and epigenetic analysis techniques have provided important information to help clarify the causes of diseases. The application of cell therapy in regenerative medicine is expected to be useful for the treatment of many types of diseases. Genetic, epigenetic, and proteomic analysis techniques play an important role in inducing the differentiation of cells used for cell therapy. Several papers focusing on the MSCs involved in the treatment of liver diseases have been published and the functions of the factors identified in the latest analysis have been explained.

A proteomic analysis using LC-MS/MS provides evidence to support the possible application of cell therapy using MSCs and information regarding the potential application of MSCs in the treatment of liver disease. This information provides important clues for investigating the function. However, MSCs are distributed throughout the body, and there are different types of MSCs, such as mesenchymal stem cells from adipose tissue (MSC-ATs), bone marrow (MSC-BMs), umbilical cord blood (MSC-UCs), and dental pulp (MSC-DPs). In previous reports, to identify the proteins expressed in MSCs, MSC-BMs, components contained in the culture supernatant of MSC-DPs and MSC-ATs were examined^{8,10,11}. Banas et al. showed that hMSC-AT secreted interleukin (IL)-1 receptor antagonist (IL-1RA), IL-6, IL-8, and granulocyte colony-stimulating factor (G-CSF), granulocyte-macrophage colony-stimulating factor (GM-CSF), monocyte chemotactic protein 1 (MCP-1), nerve growth factor (NGF), and HGF using a protein-array analysis⁸. The authors explained that these factors were effective in improving the mouse liver function. Poll et al. showed that the analysis of the serum levels of pro-inflammatory cytokines, which are known to be upregulated during liver injury, revealed a nonsignificant decrease in the levels of IL-1 and significantly lower levels of TNF- α and IL-6 after MSC-CM treatment. On the other hand, the levels of IL-10 (an anti-inflammatory cytokine) were increased four-fold in MSC-CM-treated animals. These data suggest that the infusion of MSC-CM alters the systemic cytokine profile associated with acute liver failure to a more anti-inflammatory state¹¹. Yukawa et al. reported that the administration of mouse MSC-ATs into the blood resulted in an improvement of the liver function and a reduction in the blood concentrations of TNF- α , IL-1 β and IL-6 in mice³⁷. The authors cited a paper that reported that IL-6 is

effective for improving the liver function of mice among these factors and explained the improvement of the liver function of MSC-CM³⁸. Parekkadan et al. reported that the majority (69/174 [30%]) of proteins contained in MSC-BM-CM (according to a protein array) are chemokines and are widely involved in immune regulation and liver regeneration¹¹. Similarly to the abovementioned studies, hMSC-AT-CM was also shown to improve mouse liver function (Fig. 3(a) and (b)). This study showed that hMSC-AT-CM was administered to mice to ameliorate the symptoms of acute liver failure induced by the administration of CCL4. Our findings indicate that hMSC-AT-CM is likely to have the effect of ameliorating symptoms of human liver disease. Therefore, the MSCGM-CD mesenchymal stem cell Bullet-Kit (Lonza) was used to create hMSC-AT-CM. This medium was a clinical grade medium approved by the Japanese Ministry of Health, Labor and Welfare for use in human clinical treatment research. However, we must bear in mind that the components and amounts of hMSC-AT-CM secreted by hMSC-ATs will likely change depending on the composition of the culture medium.

Since the data in the present study were obtained from the hMSC-AT-CM from one donor, we must consider the reliability of the data. In addition, the proteins were detected by a label-free method. Protein quantification was determined from the peptide ion data obtained by mass spectrometry using the number of peptide fragments identified by the database analysis as an index. This principle is based on the PAI³⁹ method, which states that, “quantitatively more proteins can detect more peptide fragments in the same protein.” This method was used to determine the emPAI⁴⁰, which estimates the protein abundance based on the peptides calculated and theoretically observed tryptic peptides for each protein using the Scaffold software program. This program identifies and quantitatively displays proteins using proprietary algorithms (Peptide/Protein Prophet, Protein grouping). Thus, the quantification of the amount of protein in this paper is a theoretical value estimated based on the emPAI⁴⁰ function of the Scaffold software program. The ratio of the number of measured peptides to the number of theoretical peptides is linearly related to the logarithm of the protein concentration, and the number obtained by subtracting 1 from the index of the peptide number ratio was defined as the emPAI⁴⁰. The larger the emPAI⁴⁰ value, the greater the amount of protein. Proteins quantified using emPAI were listed from the top in the tables showing the GO analysis results (Tables 1, 3, and 4) in descending order of concentration.

Conclusions

In this study, which used an LC-MS/MS measuring system, we focused on the quantified amount of protein and components contained in hMSC-AT-CM that improve the liver function, with a focus on the function of proteins classified by a GO analysis. These analyses revealed a number of new

candidates associated with growth (SAP, SEM7A, PTK7); the immune system processes (CO1A2, CO1A1, CATB, TSP1, GAS6, PTX3, C1 S, SEM7A, G3P, PXDN, SRCRL, CD248, SPON2, ENPP2, CD109, CFAB, CATL1, MFAP5, MIF, CXCL5, ADAM9, CATK); and reproduction (MMP2, CATB, FBLN1, SAP, MFGM, GDN, CYTC). MSC-CM contains proteins secreted by MSCs and the proteins that were initially added to the culture medium. In Table 6, the proteins identified in hMSC-AT-CM are listed in the far-left column, with the medium component proteins using culture medium for hMSC-ATs listed in the next column. Proteins secreted by hMSC are predicted by the following formula: hMSC-AT-CM containing protein – medium containing protein = hMSC-AT secreted protein. Table 6 also lists eight articles that can be searched using the keywords MSC, ADSC, mesenchymal stem cell, LC/MS/MS, CM, conditional medium, protein, and secretion on the PubMed database (<https://www.ncbi.nlm.nih.gov/pubmed/>). Secreted proteins of MSCs are listed in Table 6. This research method differs from a protein array and enables a comprehensive analysis of the protein expression. We succeeded in identifying 106 types of novel proteins contained in MSC-CM. The newly identified protein components contained in hMSC-AT-CM provide valuable information to support the clinical application of hMSC-AT-CM.

Acknowledgements

We thank Naomi Kakazu (University of the Ryukyus) for clerical assistance and Saki Uema, Yuka Onishi, Maki Higa, Youichi Toyokawa, Yuki Kawahira and Saori Adaniya (University of the Ryukyus) for providing technical support. We thank Masayoshi Tsukahara (Kyowa Hakko Kirin Co., Ltd.) for his expert technical advice on cell culture methods, which was provided under a cooperative research contract with Kyowa Hakko Kirin Co., Ltd.

Ethical Approval

Ethical Approval is not applicable for the article. (In this paper, we did not conduct clinical studies that required Institutional review).

Statement of Human and Animal Rights

All experimental protocols were performed according to the guidelines for the care and use of laboratory animals set by Research Laboratory Center, Faculty of Medicine, and the Institute of Animal Experiments, Faculty of Medicine, University of the Ryukyus (Okinawa, Japan). The experimental protocol was approved by the Committee on Animal Experiments of University of the Ryukyus (permit number: A2017101).

Statement of Informed Consent

Statement of Informed Consent is not applicable for the article.


Declaration of Conflicting Interests

The authors declared no potential conflicts of interest with respect to the research, authorship, and/or publication of this article.

Funding

The authors disclosed receipt of the following financial support for the research, authorship, and/or publication of this article: This work was supported in part by the Japan Society for the Promotion of Science (JSPS; KAKENHI Grant Number 16H07094), Japan Agency for Medical Research and Development, The Naito Foundation, and Okinawa Science and Technology Promotion Center (OSTC). This work was supported by the Research Laboratory Center, Faculty of Medicine, and the Institute for Animal Experiments, Faculty of Medicine, University of the Ryukyus.

ORCID iD

Hirofumi Noguchi  <http://orcid.org/0000-0002-0880-6805>

Supplemental Material

Supplemental material for this article is available online.

References

1. Thomas MB, Zhu AX. Hepatocellular carcinoma: The need for progress. *J Clin Oncol*. 2005;23(13):2892–2899.
2. Pittenger MF, Mackay AM, Beck SC, Jaiswal RK, Douglas R, Mosca JD, Moorman MA, Simonetti DW, Craig S, Marshak DR. Multilineage potential of adult human mesenchymal stem cells. *Science*. 1999;284(5411):143–147.
3. Bieback K, Kern S, Kluter H, Eichler H. Critical parameters for the isolation of mesenchymal stem cells from umbilical cord blood. *Stem Cells*. 2004;22(4):625–634.
4. In't Anker PS, Scherjon SA, Kleijburg-van der Keur C, de Groot-Swings GM, Claas FH, Fibbe WE, Kanhai HH. Isolation of mesenchymal stem cells of fetal or maternal origin from human placenta. *Stem Cells*. 2004;22(7):1338–1345.
5. Zuk PA, Zhu M, Mizuno H, Huang J, Futrell JW, Katz AJ, Benhaim P, Lorenz HP, Hedrick MH. Multilineage cells from human adipose tissue: Implications for cell-based therapies. *Tissue Eng*. 2001;7(2):211–228.
6. Zuk PA, Zhu M, Ashjian P, De Ugarte DA, Huang JI, Mizuno H, Alfonso ZC, Fraser JK, Benhaim P, Hedrick MH. Human adipose tissue is a source of multipotent stem cells. *Mol Biol Cell*. 2002;13(12):4279–4295.
7. Schaffler A, Buchler C. Concise review: Adipose tissue-derived stromal cells – basic and clinical implications for novel cell-based therapies. *Stem Cells*. 2007;25(4):818–827.
8. Banas A, Teratani T, Yamamoto Y, Tokuhara M, Takeshita F, Osaki M, Kawamata M, Kato T, Okochi H, Ochiya T. Ifats collection: In vivo therapeutic potential of human adipose tissue mesenchymal stem cells after transplantation into mice with liver injury. *Stem Cells*. 2008;26(10):2705–2712.
9. Osugi M, Katagiri W, Yoshimi R, Inukai T, Hibi H, Ueda M. Conditioned media from mesenchymal stem cells enhanced bone regeneration in rat calvarial bone defects. *Tissue Eng Part A*. 2012;18(13–14):1479–1489.
10. van Poll D, Parekkadan B, Cho CH, Berthiaume F, Nahmias Y, Tilles AW, Yarmush ML. Mesenchymal stem cell-derived molecules directly modulate hepatocellular death and regeneration in vitro and in vivo. *Hepatology*. 2008;47(5):1634–1643.
11. Parekkadan B, van Poll D, Suganuma K, Carter EA, Berthiaume F, Tilles AW, Yarmush ML. Mesenchymal stem cell-derived molecules reverse fulminant hepatic failure. *Plos One*. 2007;2(9):e941.
12. Nakashima Y, Miyagi-Shiohira C, Kobayashi N, Saitoh I, Watanabe M, Noguchi H. A proteome analysis of pig pancreatic islets and exocrine tissue by liquid chromatography with tandem mass spectrometry. *Islets*. 2017;9(6):159–176.
13. Pocsfalvi G, Stanly C, Fiume I, Vekey K. Chromatography and its hyphenation to mass spectrometry for extracellular vesicle analysis. *J Chromatogr A*. 2016;1439:26–41.
14. Park JO, Choi DY, Choi DS, Kim HJ, Kang JW, Jung JH, Lee JH, Kim J, Freeman MR, Lee KY, Gho YS, Kim KP. Identification and characterization of proteins isolated from microvesicles derived from human lung cancer pleural effusions. *Proteomics*. 2013;13(14):2125–2134.
15. Little KM, Smalley DM, Harthun NL, Ley K. The plasma microparticle proteome. *Semin Thromb Hemost*. 2010;36(8):845–856.
16. Wisniewski JR, Zougman A, Nagaraj N, Mann M. Universal sample preparation method for proteome analysis. *Nat Methods*. 2009;6(5):359–362.
17. Nesvizhskii AI, Keller A, Kolker E, Aebersold R. A statistical model for identifying proteins by tandem mass spectrometry. *Anal Chem*. 2003;75(17):4646–4658.
18. Wu TT, Wu SS, Ouyang GL. Periostin: A new extracellular regulator of obesity-induced hepatosteatosis. *Cell Metabolism*. 2014;20(4):562–564.
19. Lu Y, Liu X, Jiao Y, Xiong X, Wang E, Wang X, Zhang Z, Zhang H, Pan L, Guan Y, Cai D, Ning G, Li X. Periostin promotes liver steatosis and hypertriglyceridemia through downregulation of pparalpha. *J Clin Invest*. 2014;124(8):3501–3513.
20. Zhou Z, Xu MJ, Gao B. Hepatocytes: A key cell type for innate immunity. *Cell Mol Immunol*. 2016;13(3):301–315.
21. De Minicis S, Rychlicki C, Agostinelli L, Saccomanno S, Trozzi L, Candelaresi C, Bataller R, Millan C, Brenner DA, Vivarelli M, Mocchegiani F, Marzoni M, Benedetti A, Svegliati-Baroni G. Semaphorin 7a contributes to tgf-beta-mediated liver fibrogenesis. *Am J Pathol*. 2013;183(3):820–830.
22. Soto-Gutierrez A, Navarro-Alvarez N, Caballero-Corbalan J, Tanaka N, Kobayashi N. Endoderm induction for hepatic and pancreatic differentiation of es cells. *Acta Med Okayama*. 2008;62(2):63–68.
23. Lanzoni G, Oikawa T, Wang YF, Cui CB, Carpino G, Cardinale V, Gerber D, Gabriel M, Dominguez-Bendala J, Furth ME, Gaudio E, Alvaro D, Inverardi L, Reid LM. Concise review: Clinical programs of stem cell therapies for liver and pancreas. *Stem Cells*. 2013;31(10):2047–2060.
24. de Jong IEM, van Leeuwen OB, Lisman T, Gouw ASH, Porte RJ. Repopulating the biliary tree from the peribiliary glands. *Bba-Mol Basis Dis*. 2018;1864(4):1524–1531.
25. Walter MN, Wright KT, Fuller HR, MacNeil S, Johnson WE. Mesenchymal stem cell-conditioned medium accelerates skin

- wound healing: An in vitro study of fibroblast and keratinocyte scratch assays. *Exp Cell Res.* 2010;316(7):1271–1281.
26. Mao Y, Schwarzbauer JE. Fibronectin fibrillogenesis, a cell-mediated matrix assembly process. *Matrix Biol.* 2005;24(6):389–399.
 27. To WS, Midwood KS. Plasma and cellular fibronectin: Distinct and independent functions during tissue repair. *Fibrogenesis Tissue Repair.* 2011;4:21.
 28. Jang YJ, An SY, Kim JH. Identification of mfge8 in mesenchymal stem cell secretome as an anti-fibrotic factor in liver fibrosis. *BMB Rep.* 2017;50(2):58–59.
 29. Kim PH, Na SS, Lee B, Kim JH, Cho JY. Stanniocalcin 2 enhances mesenchymal stem cell survival by suppressing oxidative stress. *BMB Rep.* 2015;48(12):702–707.
 30. Heo SC, Lee KO, Shin SH, Kwon YW, Kim YM, Lee CH, Kim YD, Lee MK, Yoon MS, Kim JH. Periostin mediates human adipose tissue-derived mesenchymal stem cell-stimulated tumor growth in a xenograft lung adenocarcinoma model. *Biochim Biophys Acta.* 2011;1813(12):2061–2070.
 31. Matsuzawa M, Arai C, Nomura Y, Murata T, Yamakoshi Y, Oida S, Hanada N, Nakamura Y. Periostin of human periodontal ligament fibroblasts promotes migration of human mesenchymal stem cell through the α v β 3 integrin/fak/pi3k/akt pathway. *J Periodontol Res.* 2015;50(6):855–863.
 32. Jang YO, Cho MY, Yun CO, Baik SK, Park KS, Cha SK, Chang SJ, Kim MY, Lim YL, Kwon SO. Effect of function-enhanced mesenchymal stem cells infected with decorin-expressing adenovirus on hepatic fibrosis. *Stem Cells Transl Med.* 2016;5(9):1247–1256.
 33. Clarke MR, Imhoff FM, Baird SK. Mesenchymal stem cells inhibit breast cancer cell migration and invasion through secretion of tissue inhibitor of metalloproteinase-1 and-2. *Mol Carcinogen.* 2015;54(10):1214–1219.
 34. Liang HL, Hou HY, Yi W, Yang GD, Gu CH, Lau WB, Gao EH, Ma XL, Lu ZF, Wei XF, Pei JM, Yi DH. Increased expression of pigment epithelium-derived factor in aged mesenchymal stem cells impairs their therapeutic efficacy for attenuating myocardial infarction injury. *Eur Heart J.* 2013;34(22):1681–1690.
 35. Li F, Song N, Tombran-Tink J, Niyibizi C. Pigment epithelium-derived factor enhances differentiation and mineral deposition of human mesenchymal stem cells. *Stem Cells.* 2013;31(12):2714–2723.
 36. Liao Y, Lei J, Liu M, Lin W, Hong D, Tuo Y, Jiang MH, Xia H, Wang M, Huang W, Xiang AP. Mesenchymal stromal cells mitigate experimental colitis via insulin-like growth factor binding protein 7-mediated immunosuppression. *Mol Ther.* 2016;24(10):1860–1872.
 37. Yukawa H, Watanabe M, Kaji N, Okamoto Y, Tokeshi M, Miyamoto Y, Noguchi H, Baba Y, Hayashi S. Monitoring transplanted adipose tissue-derived stem cells combined with heparin in the liver by fluorescence imaging using quantum dots. *Biomaterials.* 2012;33(7):2177–2186.
 38. Hoek JB, Pastorino JG. Cellular signaling mechanisms in alcohol-induced liver damage. *Semin Liver Dis.* 2004;24(3):257–272.
 39. Rappsilber J, Ryder U, Lamond AI, Mann M. Large-scale proteomic analysis of the human spliceosome. *Genome Res.* 2002;12(8):1231–1245.
 40. Ishihama Y, Oda Y, Tabata T, Sato T, Nagasu T, Rappsilber J, Mann M. Exponentially modified protein abundance index (empai) for estimation of absolute protein amount in proteomics by the number of sequenced peptides per protein. *Mol Cell Proteomics.* 2005;4(9):1265–1272.
 41. Chen L, Tredget EE, Wu PY, Wu Y. Paracrine factors of mesenchymal stem cells recruit macrophages and endothelial lineage cells and enhance wound healing. *PLoS One.* 2008;3(4):e1886.
 42. Matsubara K, Matsushita Y, Sakai K, Kano F, Kondo M, Noda M, Hashimoto N, Imagama S, Ishiguro N, Suzumura A, Ueda M, Furukawa K, Yamamoto A. Secreted ectodomain of sialic acid-binding ig-like lectin-9 and monocyte chemoattractant protein-1 promote recovery after rat spinal cord injury by altering macrophage polarity. *J Neurosci.* 2015;35(6):2452–2464.
 43. Ono M, Ohkouchi S, Kanehira M, Tode N, Kobayashi M, Ebina M, Nukiwa T, Irokawa T, Ogawa H, Akaike T, Okada Y, Kurosawa H, Kikuchi T, Ichinose M. Mesenchymal stem cells correct inappropriate epithelial-mesenchyme relation in pulmonary fibrosis using stanniocalcin-1. *Mol Ther.* 2015;23(3):549–560.
 44. Aomatsu E, Takahashi N, Sawada S, Okubo N, Hasegawa T, Taira M, Miura H, Ishisaki A, Chosa N. Novel scrg1/bst1 axis regulates self-renewal, migration, and osteogenic differentiation potential in mesenchymal stem cells. *Sci Rep.* 2014;4:3652.